Measurement and performance evaluation of triple band differential integrated extraoral rectifying antenna for data transfer and RF energy harvesting for tongue drive system

scientific reports

Check for updates

OPEN

Measurement and performance evaluation of triple band differential integrated extraoral rectifying antenna for data transfer and RF energy harvesting for tongue drive system

Sarita Ahlawat[1], Binod Kumar Kanaujia[1,2], Neeta Singh[3], Aijaz M. Zaidi[2], Karumudi Rambabu[4] & Ladislau Matekovits[5,6,7]✉

Wearable assistive devices are vitally important for tetraplegic individuals to provide valuable insights into their intended directives tailored to tongue motions in wireless healthcare industries. The flexible differentially driven extraoral antenna and rectenna measurement system are developed to enable differential sensing and monitoring of the set of unique tongue gestures for extraoral tongue drive system (eTDS) applications in three frequency bands of Industrial, Scientific, and Medical (ISM) (915.0 MHz, 2400 MHz, and 5800 MHz). The performance analysis is carried out using the heterogeneous human head model. The differential rectifier is coplanarly integrated with the differential extraoral antenna on the same 0.254 mm thin and 9.5 mm wider Rogers RT/ Duroid 6010 LM substrate. The footprint of the fabricated differential rectenna is 0.135 $\lambda_g \times$ 0.082 $\lambda_g \times$ 0.002 λ_g where the planar size of differential rectifier is 15.75 $\times$ 2.5 mm^2. The fabricated systems are situated closely to an artificial head model. The maximum conversion efficiency achieved at 2400 MHz and 5800 MHz is 83.45% and 74.8%, respectively, for 11 dBm of RF input power. Further, the link analysis, including interfacing circuit losses, was carried out theoretically at 915 MHz. Thus, the proposed differential extraoral systems can be employed to acquire and transmit the user intentions in eTDS inspired healthcare applications.

Wearable assistive technologies (ATs) are the most progressive solutions for sensing, inferring, and communicating the intentions of physically disabled people to the intended smart devices. In this era of smart technologies, they can easily interact with smart devices around them using ATs, which allows them to experience an independent and more productive life[1–8]. TDS is a very promising assistive technology due to certain capabilities of the tongue, such as its great flexibility, less fatigueness, and non-invasive access. It enables communication with nearby intended targets (such as a smartphone, computer, or powered wheelchair) using different tongue gestures[5,9,10].

Previous studies of TDS[3,4,11–16] have mainly discussed two topologies of TDS, intraoral TDS (iTDS) and extraoral TDS (eTDS), where integrated electronics are situated within and outside of the user's mouth, respectively. An eTDS configuration offers maximum unrestricted space for tongue movements within the oral cavity and minimal electromagnetic coupling of integrated electronics with oral tissues in comparison to iTDS. This device accommodates a magnetic tracer, a pair of two magnetic (HMC1043) tracking sensors, transceivers, and rechargeable batteries mounted on a headset. For sensing and decoding every tongue movement, a small magnet (positioned on the user's tongue) emits varying magnetic fields, which are monitored and acquired by

[1]School of Computational and Integrative Sciences, Jawaharlal Nehru University, New Delhi 110067, India. [2]Dr. Ambedkar National Institute of Technology Jalandhar, Jalandhar 144011, India. [3]University School of Automation & Robotics, Guru Gobind Singh Indraprastha University, Delhi, India. [4]Department of Electrical and Computer Engineering, University of Alberta, Edmonton, AB T6G 2V4, Canada. [5]Dept. of Electronics and Telecommunications Politecnico di Torino, Turin, Italy. [6]Politehnica University Timisoara, Timisoara 300223, Romania. [7]Instituto di Elettronica e di Ingegneria dell'Informazione e delle Telecomunicazioni, National Research Council of Italy, Turin 10129, Italy. ✉email:

left and right sensors situated along the user's cheeks. These field variations are further measured and processed using a control circuitry (CC2510) and a set of rechargeable battery pack. This processed field information is then wirelessly transferred to the smart electronic devices around the user with the help of an antenna, enabling users to instrument and control these devices with their self-reliance[3,4,17]. Figure 1 presents the data transfer and RF energy scavenging of eTDS headset structured device where differential rectifying antenna system can effectively sense and measure the set of unique tongue movements by utilizing differential cancellation mechanism. The differential transmitter is directly interfaced with rectifier. The differential integrated antenna is to be employed within space of differential antenna with rectifier. It will facilitate eTDS communication in.

order to transmit the sensed information and harvest the ambient RF power at the lowest (915 MHz) and two higher ISM frequencies (2400 MHz and 5800 MHz), respectively. It is highly needed for physically challenged users to overcome the internal and external noise interferences that can be better instrumented based on the differential integrated antenna and their balanced configuration.

An antenna significantly impacts the overall communication link performance of an eTDS. It becomes important to pay attention to measurement of eTDS antennas and their characterization. However, eTDS has been reported using system level studies only in[3,4]. This is the first time we have proposed a multiband extraoral antenna for eTDS applications. Although the literature has addressed some iTDS antennas and their design challenges[14–16,18]. In[14,16], iTDS antennas, working only in the ISM band, were presented. However, the multiple frequency band operation was not considered, which is essential for switching data and power transfer modes to enhance the lifetime of rechargeable batteries. In[15], dual band intraoral antennas (Patch and PIFA) were designed for the ISM bands. It was seen that the antenna detuning would be significant here due to their very narrow bandwidths and exposure to the lossy environment inside the mouth. Furthermore, these TDS related antennas operate based on single port configuration that imposes the need of extra interfacing circuitry to feed

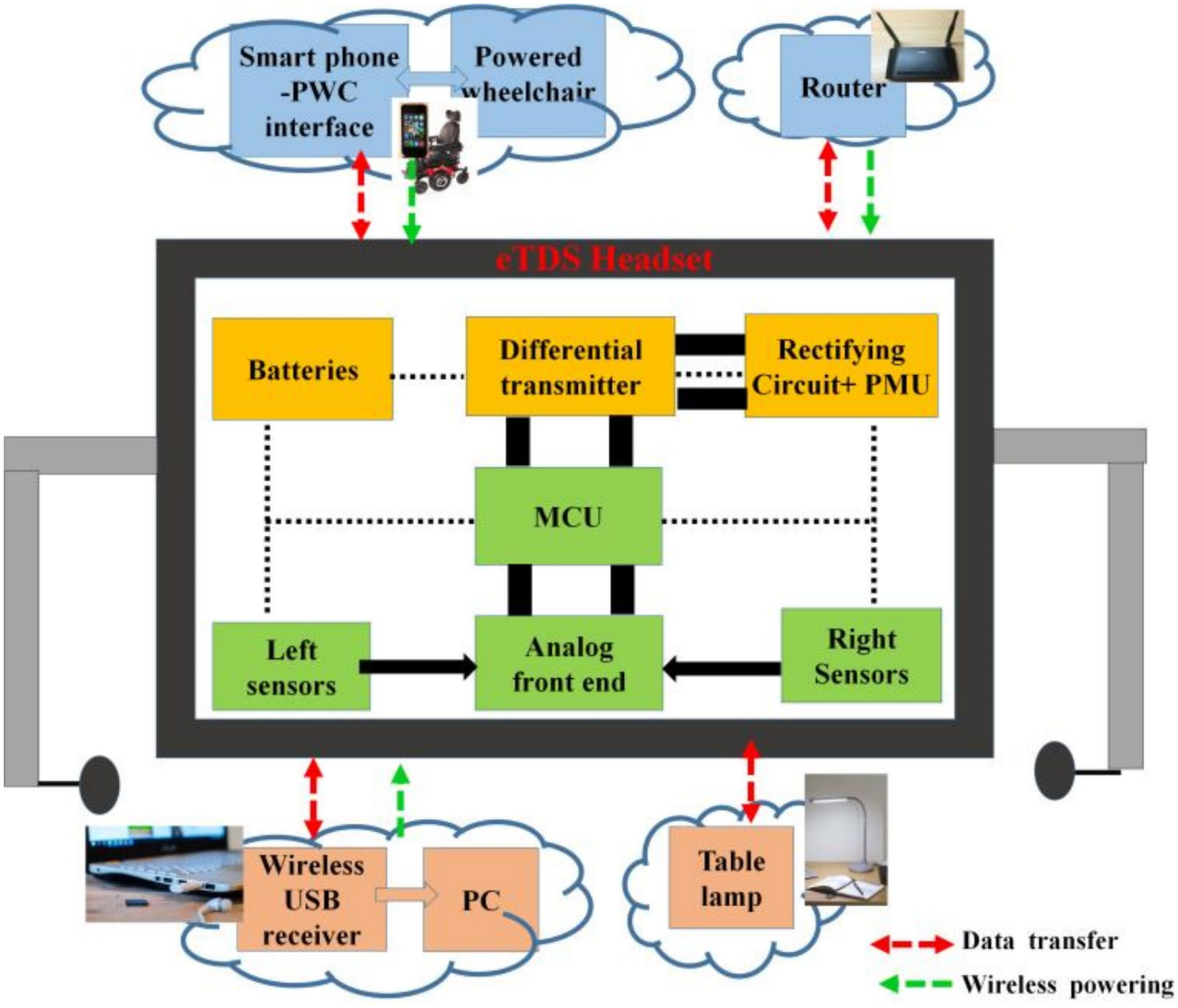

Fig. 1. Conceptual schematic of an extraoral TDS using differential rectfying system for dual mode transmission.

Ref.	[14] (2018)	[15] (2019)	[16] (2020)	[25] (2016)	[26] (2021)	[19] (2021)	[20] (2022)	[27] (2017)	[28] (2023)	[29] (2022)	[30] (2015)	[31] (2018)	Our work
Freq. (MHz)	2400	433/915	915	402/2400	2400	915/1470	915/1300	900,1800,2100	2300,3500,5700	915/2450	2450	2000,2500, 3500	915,2400,5800
Antenna type	Patch/PIFA	Dipole	Meandered Patch	Slotted Patch	Symmetrical Slotted Patch	Slotted Patch	Slotted Patch	Patch	Stacked Patch	Meandered Patch	Patch	Slotted Patch	Symmetrical Meandered Patch
TDS configuration	Arch structured iTDS	Arch structured iTDS	Arch structured iTDS	x	x	x	x	x	x	x	x	x	Headset eTDS
Area (mm^2)	60×13	42×10×2.635	20×4.4×0.025	22×23	$\pi\times5^2$	$\pi\times5^2$	8×8	200×175	50×50×66.52	5×5.25	100×70	120×120	15.75×9.5×0.254
BW (%)	18.8/29.2	7.4/11.5	163	7.4/6.6	10.2	9.8/7.34	–	~3.5	35/24.7/11.64	14.5/8.2	4.4	~1.3/2/4.1	13.04/8.61/8.89
Measured Gain (dBi)	−10.6(0)	−14.4(0)	− 17.5	− 36.7/27.1	− 27.9	— 24.62/18.3	— 19.3/17.7	8.15,7.15,8.15	8.1/8.9/9	— 22.1/19.6	5.86	7.0,5.5,9.2	– 22.36/– 13.01/– 11.93
Rad. Eff. (dBi)	x	x	x	x	x	x	— 27.1/– 26.8	x	94/96/97	x	x	85,75,72	– 28.81/– 19.36/– 8.6
Bio-compatible	Yes	Yes	Yes	*no*	Yes	Yes	Yes	No	No	Yes	No	No	Yes
Flexible	No	No	Yes	No	No	No	No	No	No	No	No	No	Yes
SAR (W/kg) (1-g/10-g avg.)	x	48.68/26.10 (10-g)	108.25 (1-g)	832/690	x	331.4/241.1 (10-g)	297.3/1.08 (10-g)	x	0.205/0.187/0.192	1.22/0.90 (1-g)	x	x	9.068/4.313/2.577
Net i/p power (dBm)	x	16.14/18.84	11.70	_	x	_	_	x	x	_	x	x	22.45/25.69/27.93
Differentially fed	No	No	No	Yes	Yes	No	No	No	No	No	Yes	Yes	Yes
Rectifier topology	x	x	x	x	x	Single	Single	Single	Single	Single	Differential	Differential	Differential
Conv. Eff. (%)	x	x	x	x	x	x/76.1	x/80.4	40	69.7 (at 2.45 GHz)	77.02/67.04	73.9	53,31,15.56	x/83.45/74.8
Rectifier area (mm^2)	x	x	x	x	x	3.4×6.7	7.0×4.0	84×35	25.3×15	_	50×40	~140×65	15.75×2.5
Rectfier directly integrated	x	x	x	x	x	No	No	No (through external SMAs)	No (through external SMAs)	No (through external SMAs)	No (through external SMAs)	No (through external SMAs)	Yes

Table 1. Comparison of differential triple band extraoral integrated antenna with previous studies. x-not considered ; - not given.

to a dual-port microcontroller unit (CC2510) of tongue drive devices which not only increase the volume of device but also increases the losses due to extra matching circuits. Although, there are few research works on two port multiple input multiple output (MIMO) antenna topology[19,20] but they are considered for capsule endoscopy applications and lack the use of differential feeding method which makes them more susceptible to external interference from the adjacent circuitry. Also, the authors have presented a full duplex implantable antenna and rectifier for seamless data and power telemetry but these units are adopted separately in a two layer configuration which can cause a key issue of the extra power consumption due to interfacing of additional connectors and matching circuits Hence, the differentially configured antennas are the good alternative for extraoral tongue drive devices to improve the measurement of data acquiring system by overcoming the space and mismatch losses.

The above discussion raises the research concern that the TDS antennas with differential feeding mechanisms have not been evaluated in earlier literature. For the first time, a differential implantable antenna working in the Medical Implant Communication Service (MICS) band (402.0-405.0 MHz) was designed in the article[21]. However, the biocompatibility parameter was not analyzed and measured. In reference[22,23], differential antennas were proposed for the ingestible capsule devices. However, these antennas were functioning in a single ISM band, which will significantly limit the battery's lifetime. Further, the reported differential antennas were mainly measured for intracranial pressure monitoring by implantable devices[21] and ingestible capsules for the gastro-intestine tract[22,23]. Here, it can be inferred that the differential antennas should be considered and evaluated for eTDS applications attributed to their direct interfacing with the microcontroller unit. Only in[24], a differential extraoral antenna is designed, operating at two ISM frequencies (0.915 GHz and 2.4 GHz) for data transmission. However, the high power consumption at analog front end of eTDS transmitter necessitates the transfer of power wirelessly based on RF energy harvesting technique.

Hence, we have proposed a first ever triple band differential extraoral integrated antenna for eTDS inspired applications. This multi-band approach will introduce simultaneous data transmission and RF energy harvesting at 915 MHz, and 2400 MHz and 5800 MHz, respectively, facilitating the eTDS device to switch their band operation concerning power availability. It can enable the efficient measurement of user's intentions by enhancing the lifetime of rechargeable batteries. It can be seen from Fig. 1 that differential rectenna integration can play a vital role in miniaturization of eTDS circuitry by facilitating the direct interfacing with neighboring circuits at the RF front end and power management unit (PMU).

RF energy harvesting is a wireless powering approach that has gained popularity for facilitating the powering of low-power electronic devices in biomedical applications due to constant advancements over Internet of Things (IoT)[2,27,28,32–35]. The communication of physically challenged users' intentions with nearby smart devices provides a better means of consuming and harvesting the freely available energies of nearby devices[36–38]. In order to efficiently harvest RF energy for use in bioelectronics, RF signals emitted through broadcasting communication supports such as WLAN, GSM, UMTS, and LTE would be useful to enable the energy harvesting and recharging whenever needed[28,39,40]. However, one problem with approach of RF energy harvesting is that the power that can be harvested is significantly constrained by the ambient RF environment's extremely low incident power density. In order to maximise the quantity of RF energy measured, a rectifying antenna (rectenna) is required to collect RF energy from various communication channels and providing the equivalent DC power. It can be inferred that the measurement of a compact and integrated rectenna capable of capturing RF energy from numerous RF sources is still to be evaluated. Although, a multi-band strategy to simultaneously process signals from many sources, resulting in an improvement in total measured DC power, has also been proposed[27,29,31,39,41,42] but none of the reported rectenna was proposed for TDS-based biomedical applications. In eTDS, AFE (Analog front end) transmits the magnetic sensors data frequently using a transmitter such as BLE (Bluetooth low energy), which consumes significant amount of power[3] and thus, multiband wireless powering approach can be one of potential solution to meet this high power consumption necessity.

With growing concern of differential structured rectennas, their unique advantages of good external noise cancellation, harmonic suppression, and easy interfacing provide the capability of aiding in the enhancement of overall efficiency of rectifying measurement unit. These rectennas are preferred to single-ended structures due to their dual port differential interfacing, eliminating the extra space for additional baluns within the tongue drive devices. In[30], a differential rectenna has been reported for Wireless Power Transmission (WPT) applications and were compared to a single-ended planar rectenna. It was observed that the differential structured one provides higher DC output. In[43], the performance of a rectifier with differential topology has been evaluated that operates at frequency of 915 MHz. It has been cascaded with a resistance compression network to overcome the variation in input impedance of rectifier. However, these rectennas have been reported only for a single operating frequency band and restricting their potential for multiple frequency band applications. In[31], a multiband differential rectenna is developed using interdigital capacitors (IDCs) for realising multi-band RF harvesting. However, the size of the differential rectenna is very large, which restricts its use for biomedical tongue drive devices. Also, the differential rectifier is measured and integrated separately, which increases the connector and interfacing losses. Therefore, we have proposed a flexible triple band differential rectenna where the rectifier is coplanarly integrated with the differential extraoral antenna on the same substrate to reduce the size of the differential rectenna measurement system, which is also a novel approach to designing an RF energy harvester for the eTDS technology-based medical applications. This differential coplanar rectenna integration will reduce the additional matching circuit, connectors, and high power consumption usage costs and losses. The upper two ISM bands (2400 MHz and 5800 MHz) are selected to enable maximum energy harvesting by utilizing the freely available RF resources and miniaturize the size of the integrated rectenna system.

In this work, a flexible triple band differentially driven extraoral antenna is presented with coplanar rectifying system. It operates at three frequency bands, 915 MHz, 2400 MHz, and 5800 MHz for data transmissions and RF energy harvesting. This is the first ever proposed extraoral differential integrated antenna system for eTDS-based

applications. The meander shaped radiator, partial ground, and two vias could offer a symmetrical configuration and significant miniaturization due to meandered electrical path length connected to the partial ground through shorting pins. The wireless telemetric link analysis is carried out to measure the capability of communication link at 915 MHz. The differential configuration of an extraoral antenna unit enhances the link performance by eliminating the extra interface and matching circuitry losses. The upper two ISM bands (2400 MHz and 5800 MHz) are selected to enable maximum energy harvesting by utilizing the two freely available resources at the corresponding frequency band in eTDS-based applications. Accordingly, the differential coplanar rectenna is also designed, and its measurement is performed. Further, the maximum permissible exposure is determined accounting to the acceptable SAR levels. The designed extraoral integrated antenna system is compared with the previous studies as presented in Table 1. To the best of the author's knowledge, this is the first-ever triple band extraoral rectenna system where the differential rectifier is directly interfaced with a differential extraoral antenna on the same plane of a substrate to reduce the size of differentially measuring rectenna, which is also a novel approach of designing RF energy harvester for the eTDS technology inspired healthcare applications.

Methodology

Simulation environment

A flexible triple band differential antenna is designed to measure the unique tongue gestures for the eTDS environment by considering the heterogeneous head model in the 3D electromagnetic simulator HFSS.18.0. It is expected that the multilayer head model should follow the dynamic head enclosure as close as possible. The relevant and realistic layers comprise of skin, muscle, tongue, teeth, and saliva enclosed within semi-cubic dimensions of $200\,mm\times$ 200 mm. Table 2 shows the electrical properties of each layer of the heterogeneous model at 915 MHz, 2400 MHz, and 5800 MHz, respectively. These electrical properties (ε_r and σ) are the averaged values of the properties dedicated to individual tissue layer at the corresponding frequencies[14,15,44]. The antenna and integrated antenna (rectenna) is placed at the top of the architectural model for eTDS independently. It is situated at a margin of 3 mm from the topmost layer of the multilayer model to respect the placement of the eTDS headset by a physically challenged subject, as shown in Fig. 2.

Design steps of the extraoral differential antenna without and with the coplanar rectifier

The single-layer extraoral integrated antenna is designed using a 0.254 mm thick Rogers RT/ Duroid 6010 LM substrate with a permittivity of 10 to justify the flexibility and biocompatibility essentials of wearable assistants. The planar dimension of the substrate is 15.75 mm x 9.5 mm and comprises of meandered rectangular patch on the top surface with a slotted ground plane on the opposite bottom surface.

The rectangular patch is meandered symmetrically about the y-axis in order to achieve the multi-band resonances. Two open-ended hook and I-structured slots are also symmetrically utilised on the bottom side plane to improve the impedance matching at the desired resonances in all three frequency bands. Two vias are inserted in each half of the top patch to follow the symmetry and obtain the desired impedance matching. We have configured two coaxial cables at a phase difference of 180° that enables the extraoral antenna to get interfaced to the planar rectifier on the same plane of the meandered patch to form a rectenna. The design process of the extraoral antenna has been carried out in Ansys 3D Electromagnetic High frequency Structure Simulator.

(HFSS 18.0) to employ triple resonances suitable for the downlink (initial assignment) and uplink (data transmission) channels of 2.4 GHz, and 5.8 GHz, and 915 MHz ISM bands, respectively. The top and bottom views of the proposed differential extraoral antenna are shown in Fig. 3.

The evolution of the proposed antenna is presented through five design steps. The differential feeding is positioned at ($\pm$ 2.4 mm, $+$ 2.7 mm) in all designing phases, as illustrated in Fig. 4. Their performance has been evaluated by dominating differential reflection coefficients, exhibited below in Fig. 5.

In Step 1, the rectangular patch is considered as the top plane of the dielectric substrate. On other side, the bottom plane is ground, as indicated. The antenna resonates at 3 GHz and 7.5 GHz and exhibits low impedance matching at both frequencies. Their resonating wavelengths are relatively close to 0.5λg and λ_g, respectively. The relevance of guided wavelength, λ_g, is counted considering the field lines are confined within the dielectric. In next Step 2, the radiating patch is miniaturized and converted into a meandered shaped patch. These meandering line transformations shifted both resonances towards lower frequencies and produced one more resonance at 1.03 GHz. All these three resonances (1.03 GHz, 2.9 GHz, and 5.7 GHz) exhibit poor impedance matching.

In Step 3, I-shaped and inverted hook slots are incorporated into the bottom ground plane results into a frequency shift to resonances at 870.0 MHz, 2.23 GHz, and 5.46 GHz in both the ISM bands, respectively. These slots lower the frequency due to the reactive capacitance effect on the differential feed impedance and

Tissues	0.915 GHz		2.4 GHz		5.8 GHz	
	ε_r	σ(S/m)	ε_r	σ(S/m)	ε_r	σ(S/m)
Skin	41.33	0.872	38.06	1.44	35.10	3.72
Muscle	54.99	0. 948	52.79	1.71	48.50	4.96
Saliva	76.00	0. 818	74.1	1.07	72.40	1.65
Tongue	55.23	0.942	52.7	1.77	47.80	5.24
Teeth	12.44	0. 145	11.4	0.385	9.67	1.15

Table 2. Dielectric properties of biological tissues.

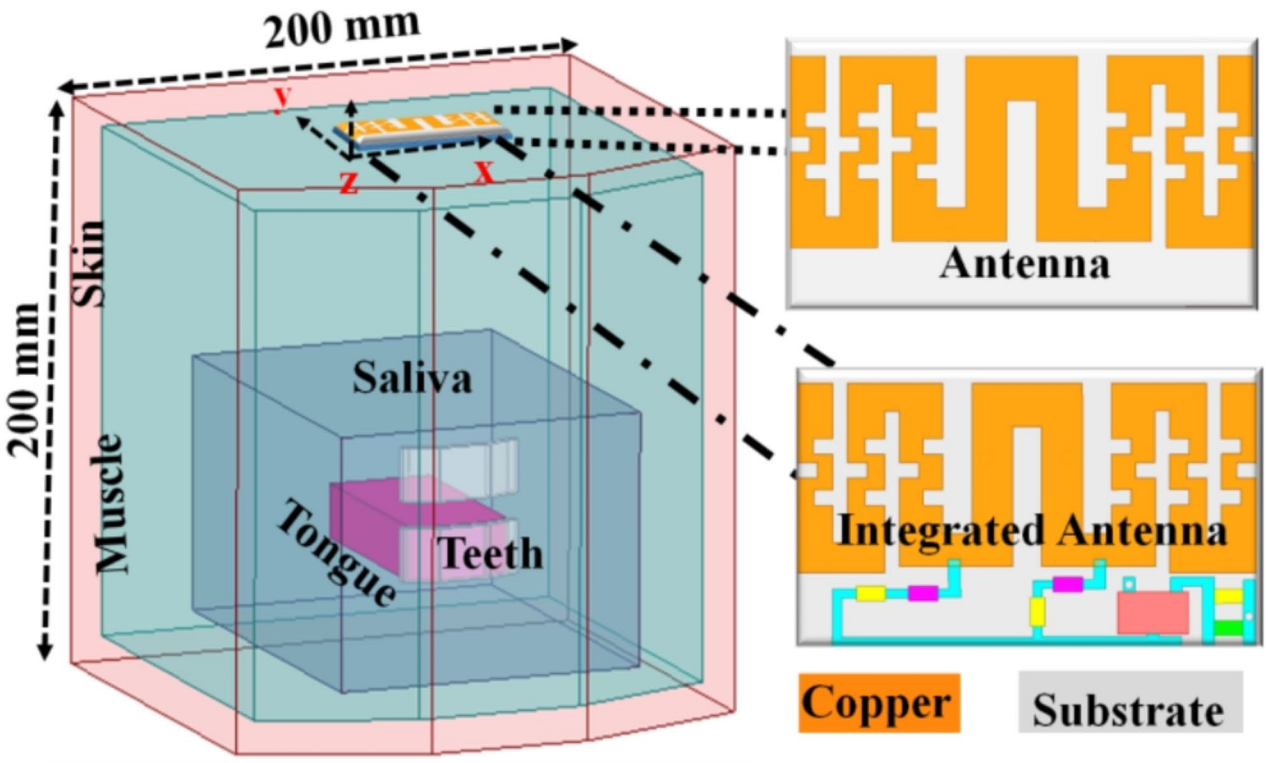

Fig. 2. Heterogeneous multilayer head model for differential measuring system.

considerably improve the input impedance matching of the extraoral antenna. In addition, two shorting pins are also symmetrically loaded in each half (± 1.4 mm, 1.1 mm) of the meander shaped patch to further tune all the resonances at the desired resonating frequencies by minimizing the capacitive effect owing to their inductive characteristics. The designed antenna thus exhibits multiple resonances at 915.0 MHz, 2400 MHz, and 5800 MHz with differential reflection coefficients of -21.08 dB, -23.02 dB, and -25.02 dB, respectively. Please note that the radiation mechanism of each resonating frequency has been validated by using surface current distributions (see Fig. 6) in the following section.

The extraoral antenna of step-3 is the final antenna selected to integrate with the rectifier on the same antenna surface to avoid connector losses and facilitate direct interfacing to form a rectenna unit. Therefore, the rectifier is designed and integrated, in the step-4, at the lower portion of the radiating patch on the same substrate, which detunes the operating frequency of the extraoral antenna. The integrated rectifier has been printed on the same plane of radiating patch as shown in Fig. 3. After that, the shorting pins/Vias and I-shaped slot are utilized to overcome the detuning effect observed due to the undesired coupling of the rectifier with an extraoral antenna. For this purpose, the parametric analysis of ground I-shaped slot size and position of vias are performed, which has been discussed in detail below in the subsection (see Section-D).

In step-5, the final proposed differential integrated antenna is obtained based on the study of design parameters associated with I-shaped slot (L_g and W_g) and Vias position (V_y) in the previous step-4. This differential rectenna integration on the same plane will eliminate the connecter losses and facilitate direct interfacing, which can also contribute to reducing the overall size of the wearable assistant.

Surface current distributions

To validate the radiating mechanism at each frequency of operation, the current distribution of the meandered patch surface is considered for the 0° phase (see Fig. 6). At 0.915 GHz, the current vector traverses from the left half to the right half in one direction. Here, the electrical length of the meander shaped radiator and the slotted ground gets merged through shorting pins to attribute the lowest frequency wavelength. It can be verified from Fig. 6a that the right half of radiating patch and most of the ground plane is activated at the lowest frequency of 915 MHz to excite the lowest frequency resonance. However, in Fig. 6b, the current vector changes direction at 2.4 GHz as it flows from the right to the left half (half wavelength mode). The traversing current length varies non-uniformly at a higher frequency due to the influence of phase change along the length of the meandered patch in each half of the patch. Similarly, at 5800 MHz, the traversing current aligns its direction more than once while moving from the left half to the right of patch (full wavelength mode), as presented in Fig. 6c.

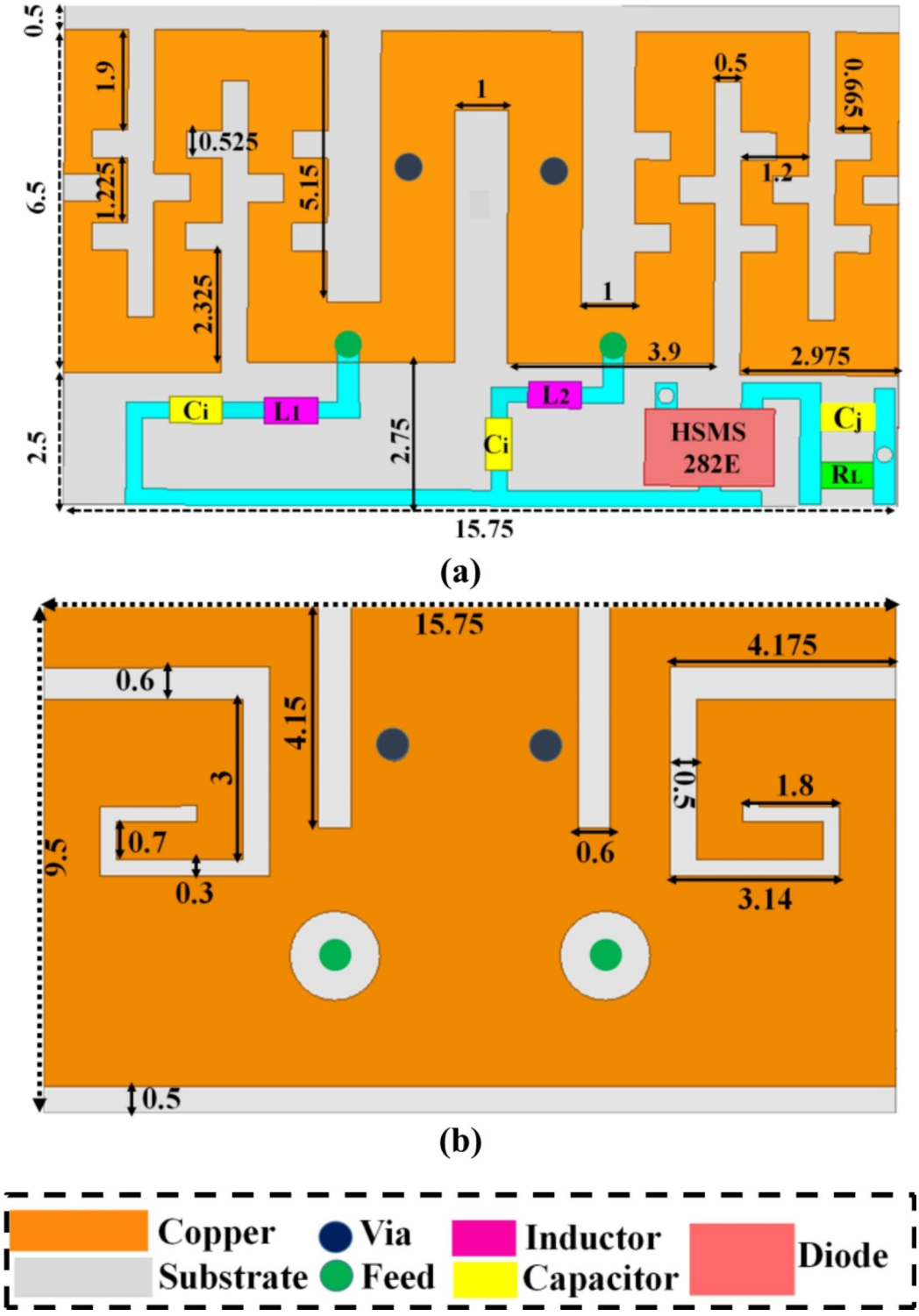

Fig. 3. Configuration of a differentially measuring extraoral integrated antenna (Units: mm) (**a**) Top side (**b**) bottom side.

Parametric study

In this section, the parametric study of designed design parameters is presented that considerably influence the nature of resonances of the designed extraoral integrated antenna. Here, this study is conducted within the same simulation head model (see Fig. 2) for different positions of shorting pins, lengths, and widths of I-shaped ground slots, as depicted below in Figs. 7, 8 and 9.

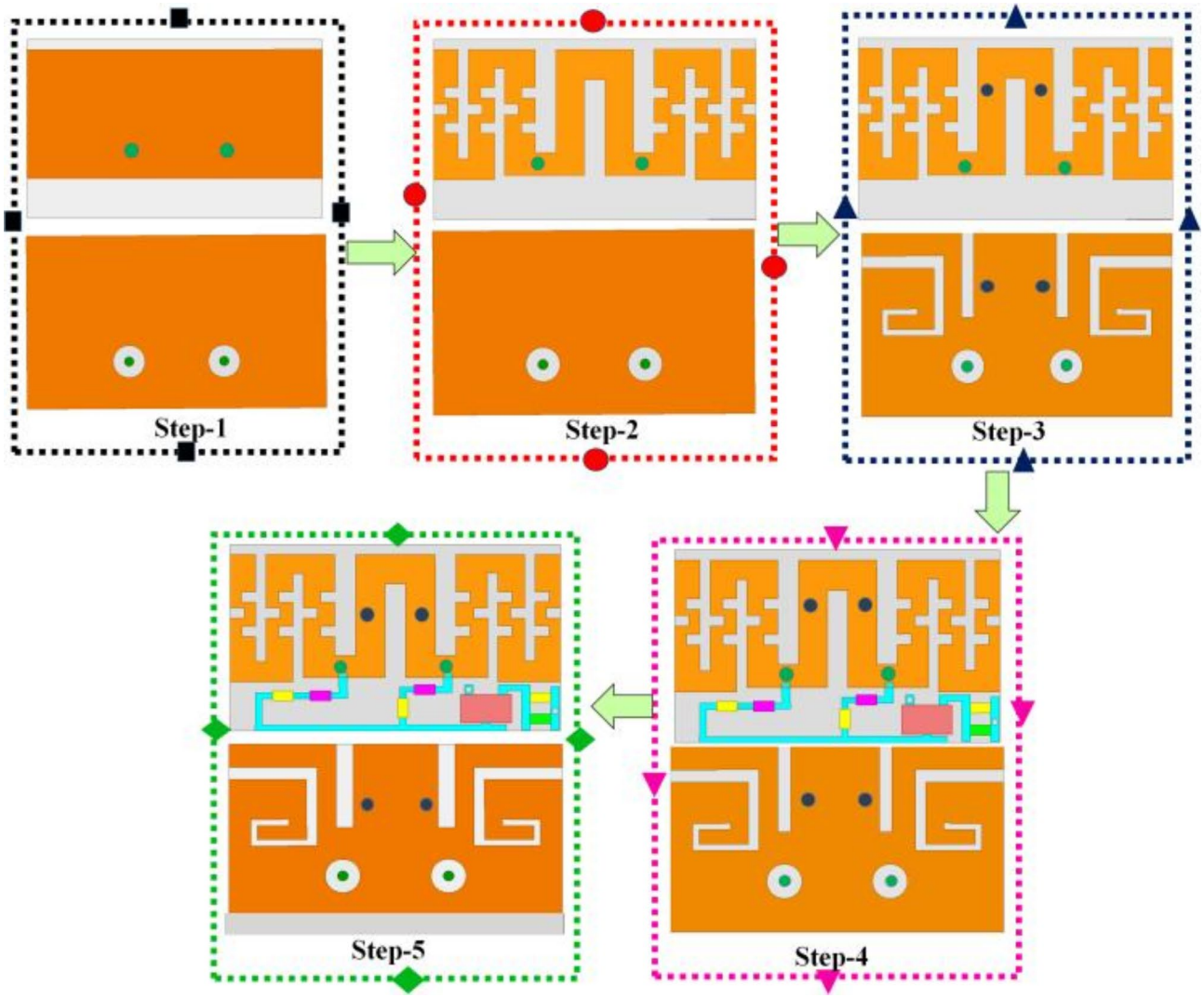

Fig. 4. Step-wise evolution of exterior differentially configured antenna and rectenna units.

Impact of length and width of I-shaped slot

The impedance matching of the differentially driven extraoral integrated antenna varies with different dimensions of the I-shaped slot. This slot plays a important role in evaluating the impedance matching. For this purpose, a parametric analysis is crried out for these parameters, L_g and W_g, given in Fig. 7. The change in differential reflection coefficient (S_{dd}) with L_g is shown in Fig. 7a. It is observed that the impedance matching of the 2400 and 5800 MHz bands improves considerably as L_g increases from 3.3 to 3.9 mm, however the impact on the 0.915 GHz resonance is insignificant. At first resonance of 0.915 GHz, Img Z_{dd} is approximates to zero at all values of L_g, and Real Z_{dd} is relatively close to 100Ω for L_g = 3.3 to 4.2 mm, shown in Fig. 7b and c. In case of the second resonance at 2400 MHz, as L_g is varied from 3.3 to 3.9 mm, impedance matching improves considerably; the differential impedance Z_{dd} is capacitive for Lg = 3.3 mm and 3.6 mm, although it is inductive for L_g = 4.2 mm and 4.5 mm. However, at L_g = 3.9 mm, Img Z_{dd} approximates to zero, and Real Z_{dd} is near to value of 100 Ω, that leads to desired matching at 2400 MHz. Furthermore, for the third resonance at 5800 MHz, the impedance is nearly capacitive at 3.3 mm and inductive at 4.5 mm. As L_g varies from 3.6 to 4.2 mm, Img Z_{dd} is approximates to zero, and Real Z_{dd} is close to value of 110 Ω. Therefore, L_g = 3.9 mm is selected as the final optmised length of the I-shaped slot where the return losses are observed at −23.01, −22.97, and −25.03 dB at 0.915, 2.400, and 5.800 GHz, respectively.32.

The deviations in S_{dd} with the change in the I-shaped slot width W_g from 0.5 to 1.3 mm are presented in Fig. 8. We can see in the Fig. 8, W_g majorly affects the impedance matching of first ISM band only. As W_g increases from 0.3 to 1.1 mm, the impedance matching of the first resonant of 0.915 GHz considerably improves and also a small drift in frequency is seen, whereas the impedance matching of second and third frequency resonance is hardly affected along with a small frequency drift, as shown in Fig. 8a. At 0.915 GHz, Img Z_{dd} is not zero for all values of W_g except for 1.1 mm, However it is capacitive at 0.3 mm and 0.5 mm, and inductive at 0.9 mm, and 1.3 mm. The value of Real Z_{dd} for W_g = 1.1 mm is 112Ω, that approximates to 100 Ω, employing good impedance matching at this frequency. In case of remaining resonances, Img Z_{dd} is nearly capacitive except at 1.1 mm for all values

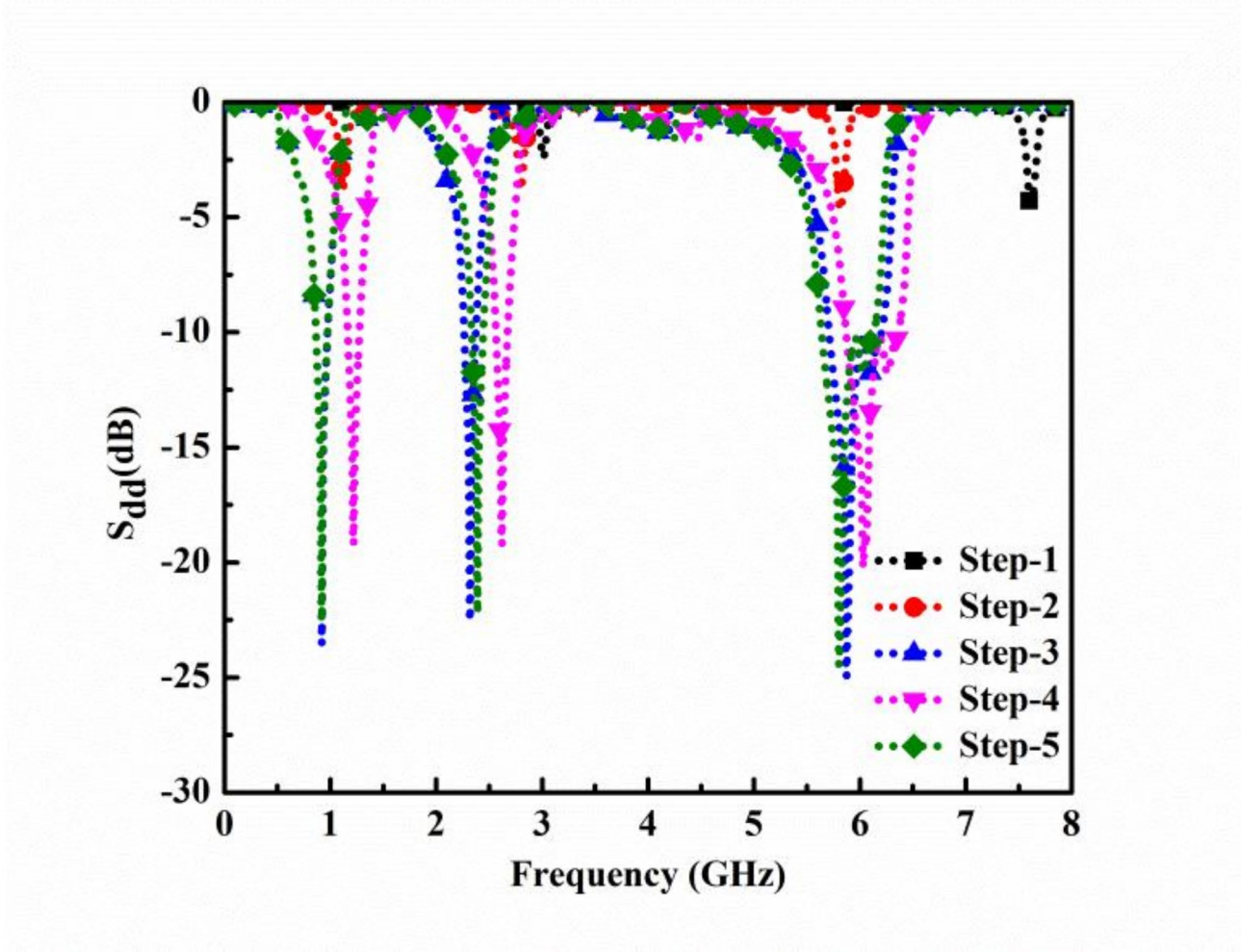

Fig. 5. Simulated differential mode coefficients $|S_{dd}|$ of each design step.

of W_g. At W_g is equal to 1.1 mm, Img Z_{dd} is zero and Real Z_{dd} is around 100 Ω (see Fig. 8b and c). So, the value of $W_g = 1.1$ mm is chosen to be the most appropriate value for slot, where return losses of − 17.01, − 23.13, and − 19.18 dB were found at 915.0 MHz, 2400 MHz, and 5800 MHz, respectively. However, the frequency tuning is sensitive to the positions of symmetrical vias which is also to be discussed in the next section.

Impact of via position

The influence of the symmetrical vias position on S_{dd} and the differential impedances of the extraoral integrated antenna is presented in Fig. 9. Here, two vias positioned symmetrically in each half of the designed antenna serve a significant role in frequency tuning at all three resonances. It is possible to see from the Fig. 9 that the imaginary half of Z_{dd} (Img Z_{dd}) is close to zero with respect to all the positions of via at 915 MHz; however, the real half of Z_{dd} (Real Z_{dd}) varies considerably for the vias position. For the via positions of V_1 and V_2, the resonances are achieved at the lower side of ISM band resonances. At position V_3, the desired resonances are achieved with the required impedance matches. The real half of differential impedance Re(Z_{dd}) is around 100Ω, and the imaginary half of differential impedance Img (Z_{dd}) is almost zero. Above V_3, the resonances at the position of vias at V_4 and V_5 have shifted to the upper side of the desired resonances due to capacitive impedance. As the position of the via moves to V_1, V_2, and V_3, the capacitive reactive impedance decreases and becomes close to zero at V_3. Above the V_3 position, the inductive reactance increases at V_4 and V_5, as presented in Fig. 9c. So, the desired location of these vias is fixed at V_3, where the return losses at 915 MHz, 2400 MHz, and 5800 MHz are − 23.5 dB, − 22.77 dB, and − 25.05 dB, respectively.

Dual band differential rectifier layout

An extraoral antenna (Step-3) evaluated at the differential impedance of 100Ω and the differentially driven dual-band rectifier should be matched. Differentially driven dual-band rectifier utilizes L-C matching network between an extraoral antenna and rectifier to accommodate and measure the maximum conversion efficiency. The fabrication of the differential rectifier has been realized on the substrate RT/Duroid 6010 ($\varepsilon_r = 10$). The dual-band differential rectifier network with the matching network is simulated and optimized using Keysight

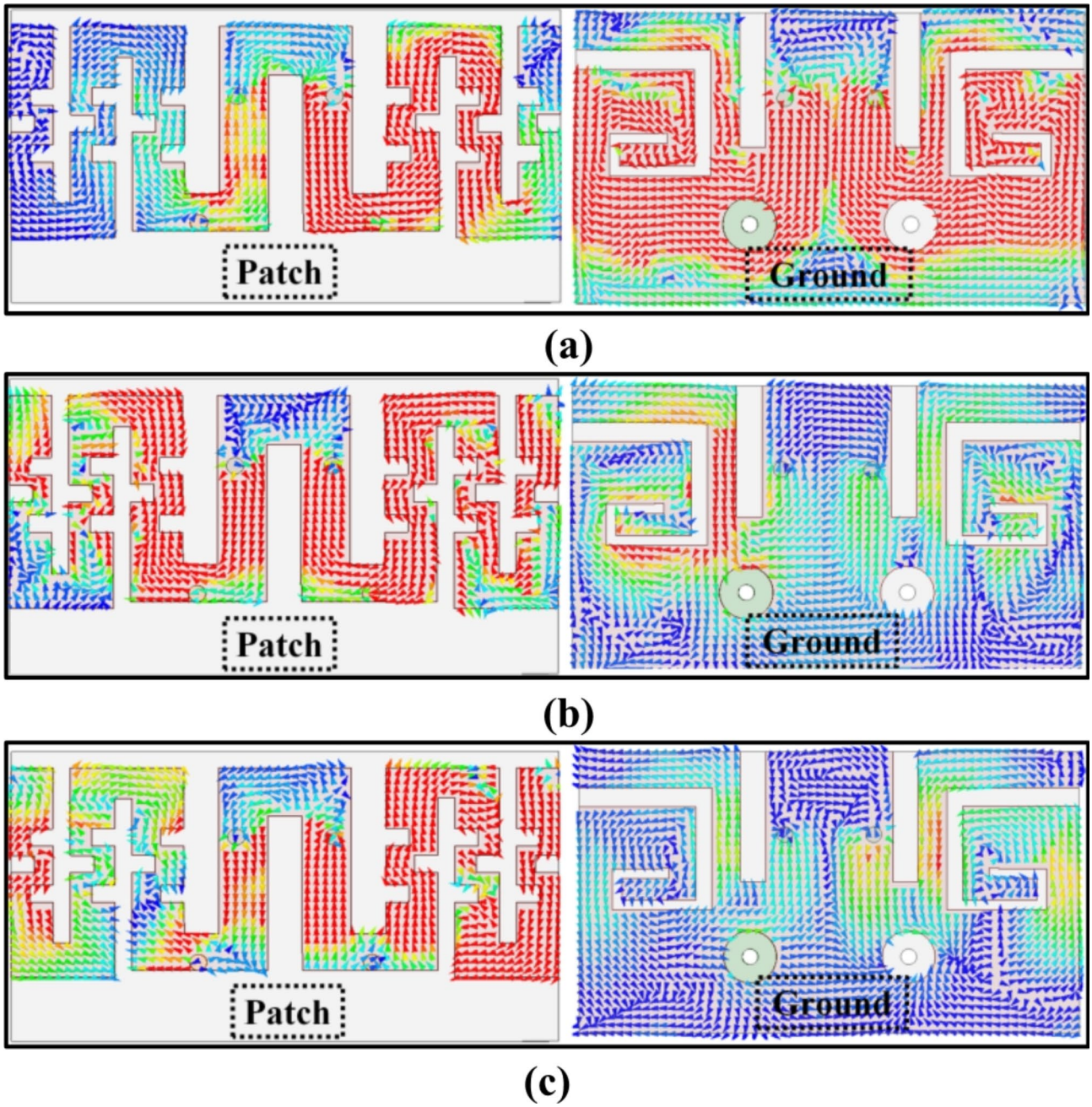

Fig. 6. Surface current distributions on the radiating patch and ground of the differentially measuring extraoral antenna (Step-3) at (**a**) 915 MHz (**b**) 2400 MHz and (**c**) 5800 MHz.

Advanced Design System (ADS) simulator. To measure and evaluate a compact rectifier design, lumped components have been utilized because the distributive components like stubs (radial and butterfly stubs) and microstrip lines require more surface area that accounts for an increase in the device volume, which is the main constraint for wearable tongue drive devices.

The designed single ended rectifier operates on two resonating frequencies, 2400 MHz and 5800 MHz. The detailed schematic circuit has been shown in Fig. 1, $L_1 = 10$nH, C_i=8pF, C_j=40nH, R_L=1KΩ. Figure 10a shows the matching network consisting of a series L-C impedance matching circuit. In which L and C work as low-pass filter and C_j act as a DC-pass filter. Two reactances of a single circuit facilitate the required two resonating frequencies[31]. Schottky diode HSMS-282E realized based on high breakdown voltage ($V_B = 7$ V) and low forward voltage ($V_F = 0.15$ V) on ADS. Voltage doubler topology, among other rectifier topologies like Greinacher, bridge, and center tap, is able to offer higher power levels[45]. To realize the intended differential circuit, the same replica of the single port rectifier has been evaluated with an 180^0 phase shift, which is presented in Fig. 10b.

Differential rectifier could generate two resonating frequencies, 2.45 GHz and 5.8 GHz same as a single port rectifier but with high conversion efficiency. The differential rectifier is designed and implemented for

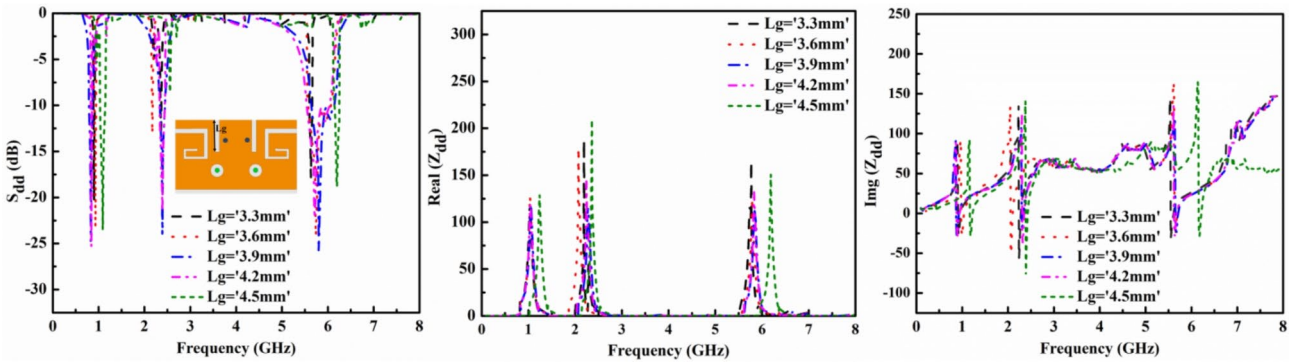

Fig. 7. Variations in the ground I-shaped slot length (**a**) S_{dd} (**b**) Real Z_{dd} (**c**) Img. Z_{dd}.

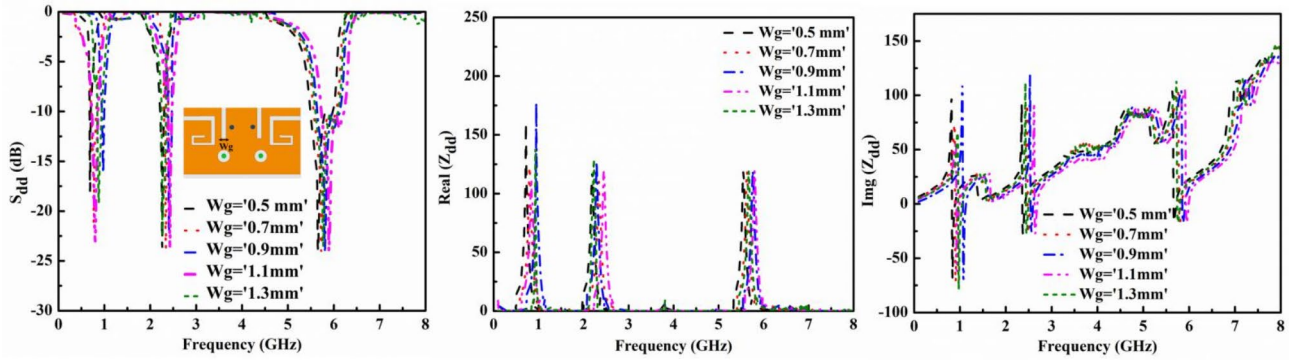

Fig. 8. Variations in the ground I-shaped slot width (**a**) S_{dd} (**b**) Real Z_{dd} (**c**) Img. Z_{dd}.

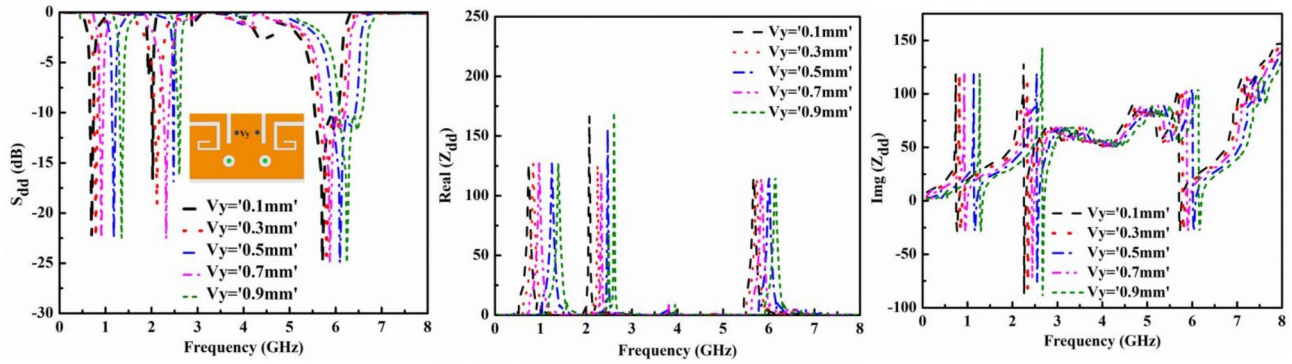

Fig. 9. Variations in the positions of symmetrical vias (**a**) S_{dd} (**b**) Real Z_{dd} (**c**) Img. Z_{dd}.

eTDS applications with parameters $L_1 = 4$nH, $L_2 = 10$nH, C_i=10pF, C_j=100pF, and Load Resistance R_L= 1KΩ. The simulated diode's impedance is 20+j26 Ω, which can be matched with 100 Ω by incorporating an LC matching network. The capacitor used in the matching circuit is the same in both branches, but the polarity of the connection is different due to differential input. Figure 10c illustrates the schematic of a fabricated prototype incorporated on the designed antenna's top surface for coplanar integration (See Step-5).

The simulated differential reflection characteristics of the rectifier have been presented for three different RF power levels of -20.0 dBm, -10.0 dBm, and 10.0 dBm at two higher frequencies, 2400 MHz and 5800 MHz, given below in Fig. 11. The differential structured rectifier is able to utilize the adjacent RF powers efficiently at both the resonating frequencies, 2400 MHz and 5800 MHz by ensuring continuous and optimum dc voltages.

Experimental near and far field- setups

A flexible and biocompatible polyimide substrate was selected to evaluate the experimental performance of the proposed differentially measuring extraoral integrated antenna (rectenna). The substrate was 0.254 mm

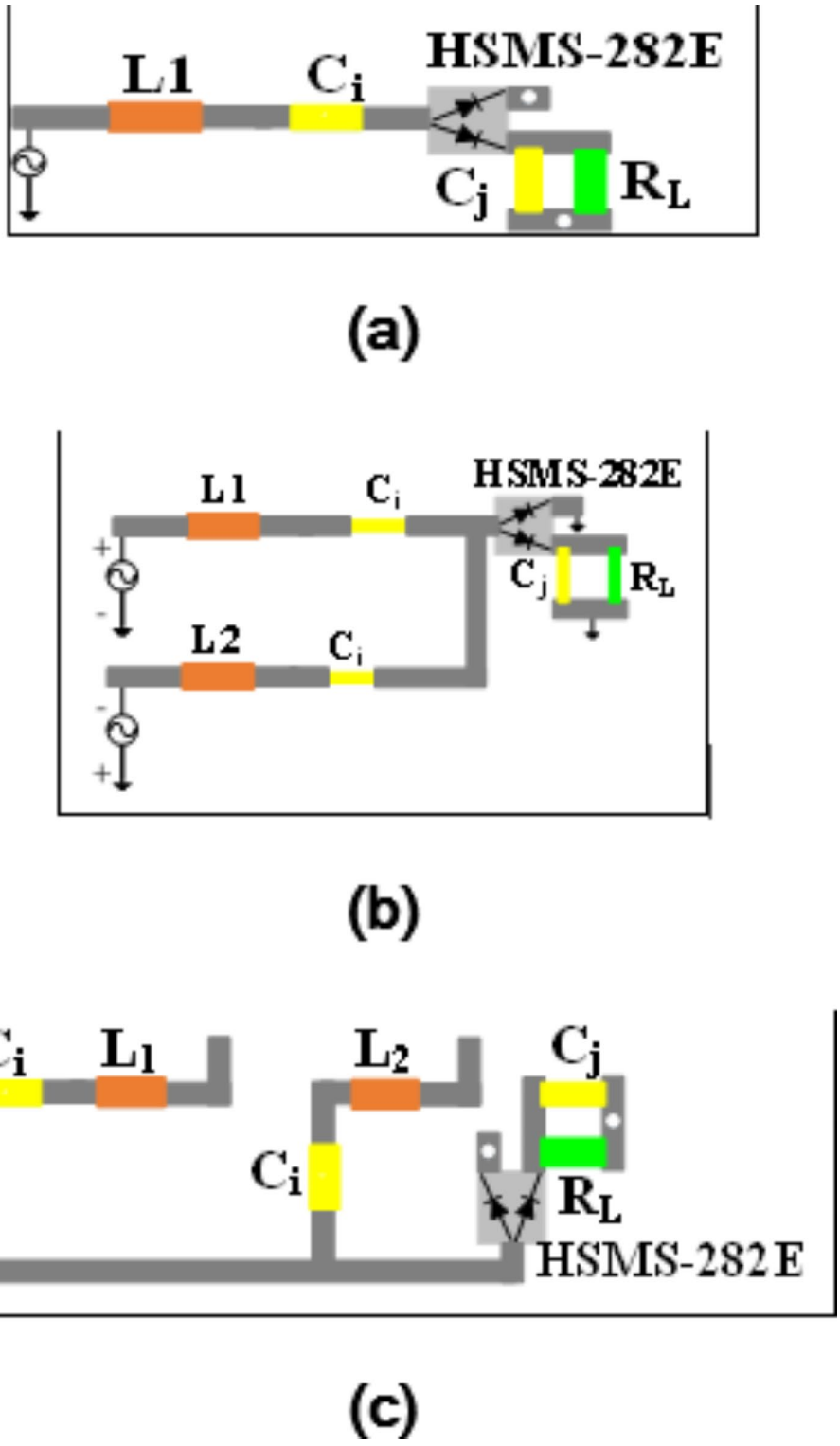

Fig. 10. (**a**) Single ended rectifier, (**b**) differentially configured rectifier, (**c**) differentially measuring rectifier interfaced with antenna (Design step-4).

thick and had a copper enclosing for upper patch and ground sides fabrication. It was preferred because of the flexibility to align with the subject's body in contact, which is essential for wearable assistive technology pertaining to eTDS. The extraoral antenna was also integrated with the rectifying circuitry on the same substrate for RF energy harvesting and sustainable inference of the user's intentions, as indicated above in Fig. 12. Initially, the extraoral differential antenna and rectenna prototypes were fabricated. The first row of Fig. 12 presents both sides (top and bottom) of fabricated antenna and rectenna. Subsequently, the lumped circuit components,

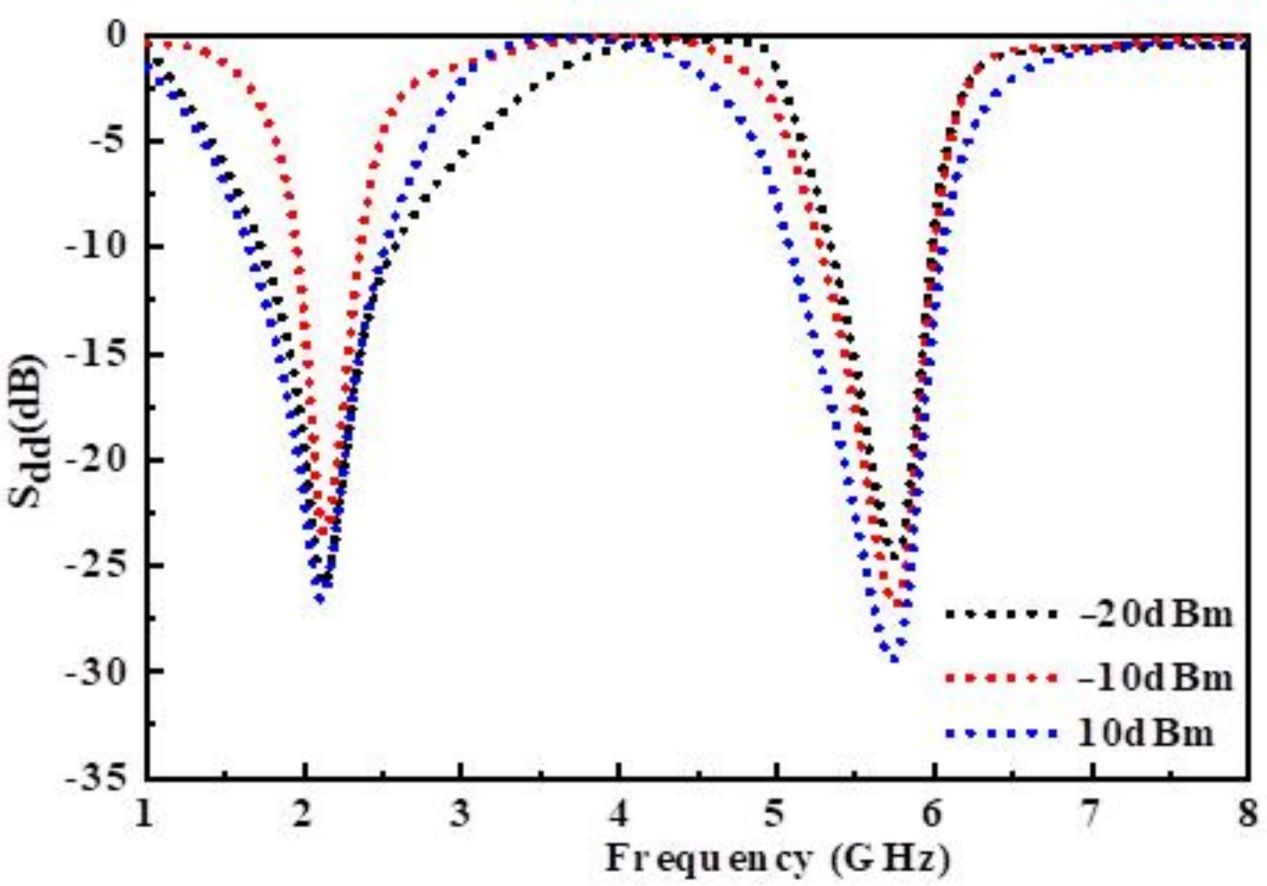

Fig. 11. Reflection coefficient (S_{dd}) of rectifier at various power levels.

such as resistors, inductors, capacitors, and Schottky diodes, were soldered onto the rectifier circuit layout. The shorting pins and differential feeding probes were soldered to achieve contact between the patch and ground of the antenna and the adjacent circuitry, as shown in the uppermost row of Fig. 12. We tracked the load resistor in end of the differential rectifier to obtain the measured DC output voltage. These sequence-wise fabrication steps are presented in the Fig. 12. Afterward, these prototypes are positioned closely at upper surface of an artificial 3D human head model to validate its near and far-field measurements, as shown in Fig. 12.

The experimental setup used to measure the scattering parameters is presented in Fig. 12. A pair of 50-Ω coaxial cables were required to connect the proposed differential antenna and rectenna prototypes to a VNA (Anritsu MS2038C) to measure the differential reflection coefficient within the frequency spectrum of 0–8 GHz. The VNA was connected to input terminal of Balun (BAL006) through calibrated front panel testing cable and the output dual ports are coupled to the proposed differential antenna and rectenna individually. The far field experimental setup is presented above in Fig. 12, where an RF signal generator was connected to a transmitting horn antenna to transmit the power to receiving extraoral antenna and rectenna systems. The measurement system adopts the balun to transform the receiving differential input to one outgoing signal, which will be fed to the end signal analyzer[46] (see Fig. 12b). Here, the maximum gain values of −22.9 dBi, −14.16 dBi and −12.83 dBi are obtained at 915 MHz, 2400 MHz and 5800 MHz, respectively. Here, the Friss equation is used to estimate the respective gain values. Further, the measured DC voltage (V_{dc}) values are retrieved across the load resistor (R_L) to corresponding received powers of the rectenna circuit using two probes and a voltmeter, as shown in Fig. 12b[47]. As aforementioned, an interface (balun) is adopted only for measurement purpose. This is not required for actual eTDS application as the AUT is well suitable for direct interface with the neighboring driving circuitry, such as microcontroller and rectifier systems. Please note that the corresponding measured results of both field setups are presented below in the following section.

Results and validation

Differential reflection coefficients

The simulated and measured near field results of differentially configured extraoral antenna and integrated antenna systems are illustrated in Fig. 13. Here, $|S_{dd}|$ indicates the dominating differential mode reflection coefficients. In simulation model, the designed antenna shows that the resonances at 915 MHz, 2400 MHz, and 5800 MHz and have impedance bandwidth from 860 MHz to 980 MHz (13.04%), 2300 MHz to 2500 MHz (8.61%) and 5700 MHz to 6230 MHz(8.89%), respectively. In the measured result, the impedance bandwidth is

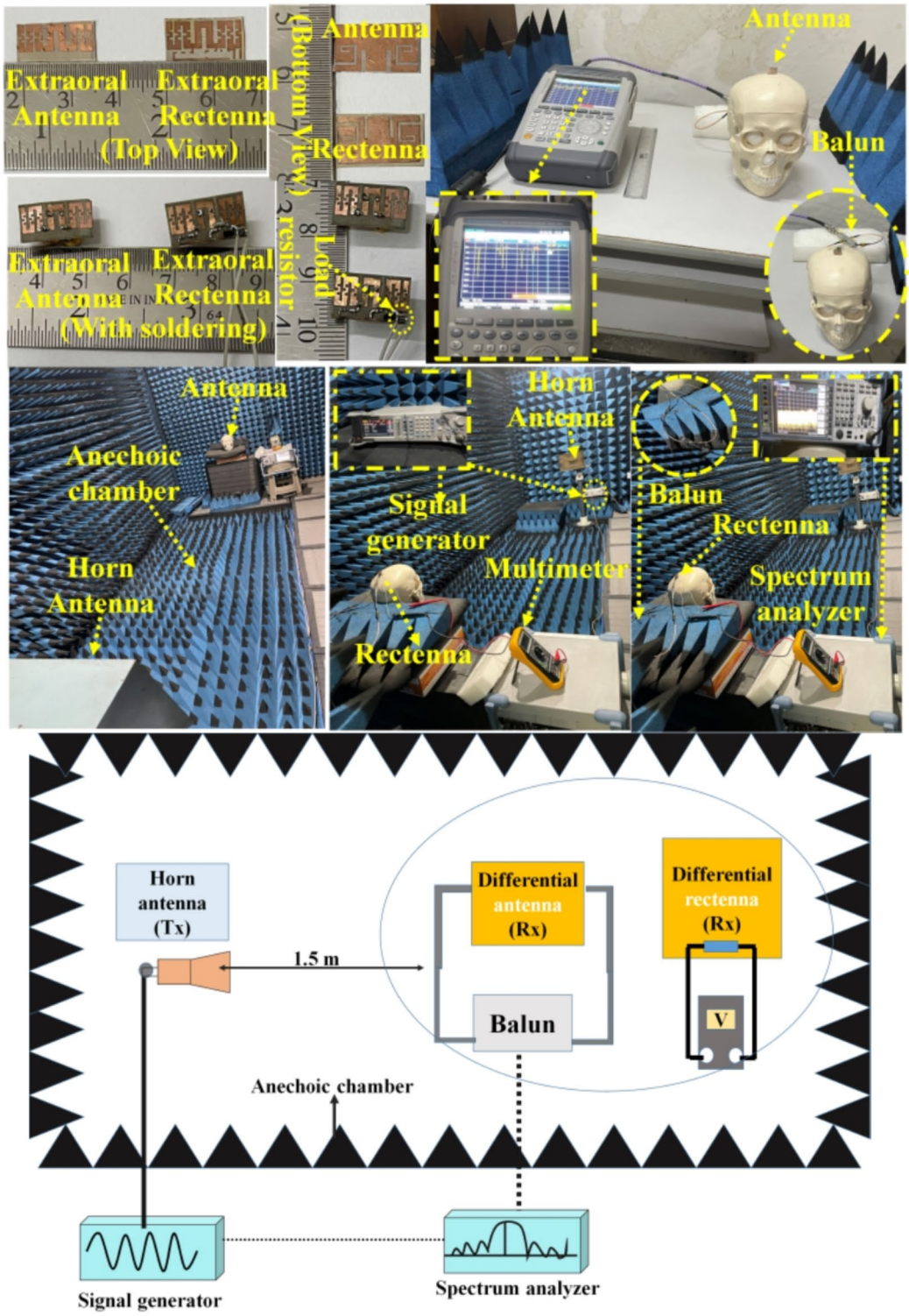

Fig. 12. (**a**) Fabricated antenna and rectenna tested within the near and far-field measurement setups (**b**) their schematic for far-field measurement system.

exactly close to the simulated bandwidth except at the highest resonance, 5800 MHz. The measured bandwidth is from 5630 MHz to 5960 MHz (5.67%) with small errors, which could be possible due to fabrication errors and measurement accessories. Similarly, the measured results of the designed rectenna are certainly following the simulated ones attributed to the optimization done after integrating the antenna with the rectifier.

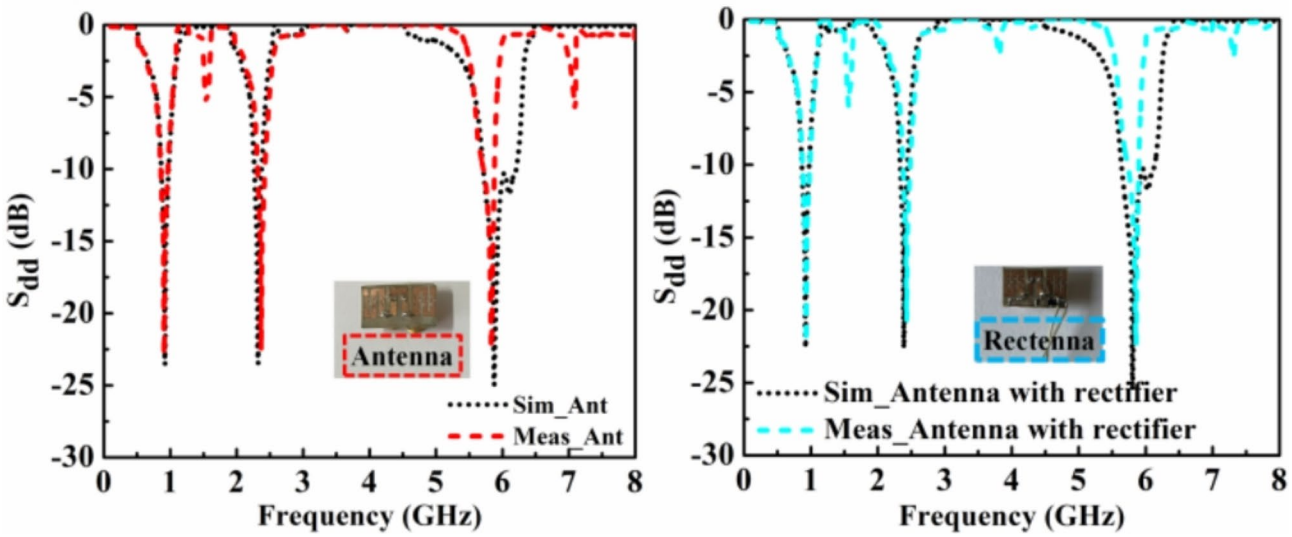

Fig. 13. Near field characteristics of the designed extraoral antenna and rectenna system (simulated and measured).

Radiation pattern and far-field gains

Figure 14 shows the comparison of measured radiation patterns of the designed integrated antenna with simulated results. It can be observed that the simulated and measured peak gain values are −22.36 dBi and −22.9 dBi, −13.01 dBi and −14.16 dBi; and, −11.93 dBi and −12.83 dBi at 915 MHz, 2400 MHz and 5800 MHz, respectively. The radiation patterns are in the off-body direction, ensuring a good TDS communication link with exterior smart electronic devices without causing any harm to the user's health. It can be seen that the radiation patterns are becoming more non-uniform at higher frequencies due to their sensitive exposure. But, the measured patterns show a similar radiation performance.

Conversion efficiency and DC output

The conversion efficiency of the differential rectifier is evaluated for two higher resonating frequencies (2400 MHz and 5800 MHz), which is important to retrieve the harvested energy in terms of the output DC voltage across the load.

$$\eta \ (\%) = \frac{V_{DC}^2}{R_L \cdot P_{in}} \times 100 \tag{1}$$

Figure 15 depicts the rectifier's conversion efficiency and output DC voltages for both resonating frequencies at an optimized load of 1KΩ. It is seen that the designed rectifier can acquire maximum efficiency at low power levels. At 5dBm, the simulated maximum conversion efficiency is 83.45% and 74.8% at 2.45 GHz and 5.8 GHz, respectively. For the input power level of 10dBm onwards, the conversion efficiency starts decreasing because the dc output voltage begins to move closer to the diode breakdown voltage of $V_B/2$ (3.5 V), as shown in Fig. 15. Further, the output DC voltages taken across the load resistor and respective calculated conversion efficiencies are obtained using Eq. (1)[34,31], where V_{DC} is the measured DC voltage and P_{in} is the input power to the differential rectifier. The designed rectenna was given 11 dBm, and the corresponding DC output voltage of 2.7 V was measured using the load resistor. For tongue drive devices, the control circuitry requires an operating voltage between 2.5 V and 3 V to sustain the inference of tongue gestures. Hence, the differential rectenna can be potentially considered to facilitate the neighboring circuitry of eTDS without depending on the battery unit.

Specific absorption rate (SAR) estimation

To evaluate the accumulation of electromagnetic radiations from the extraoral integrated antenna on the neighboring head tissues, the SAR parameter is evaluated based on the IEEE standards. Figure 16 depicts that most of the field is intensified in the vicinity of the radiating patch geometry. The SAR levels are evaluated in order to align with IEEE C95.1-1999 (1 g) standards[25] at 915 MHz, 2400 MHz, and 5800 MHz, respectively, which are 9.068 W/Kg, 4.313 W/Kg, and 2.577 W/Kg, respectively. At 915 MHz, the maximum power allowed for data telemetry is 22.45 dBm. It is important to note that although these values are calculated with respect to applied power of 1 W, real-time applications only allow for an input power of -16 dBm (ITU-R RS.1346). The major goal of maintaining such a low input power is to minimize interference between adjacent communication equipment and in/on body biomedical devices. Concerning this, the proposed antenna is secure for input power of 22.45 dBm. On the other hand, the maximum amount of power that could be incident on the extraoral antenna from freely available RF energy harvesting resources is 25.69 dBm and 27.93 dBm at 2400 MHz and 5800 MHz, respectively. According to FCC guidelines, the effective isotropic radiated power (EIRP) limit is 36 dBm for P_T

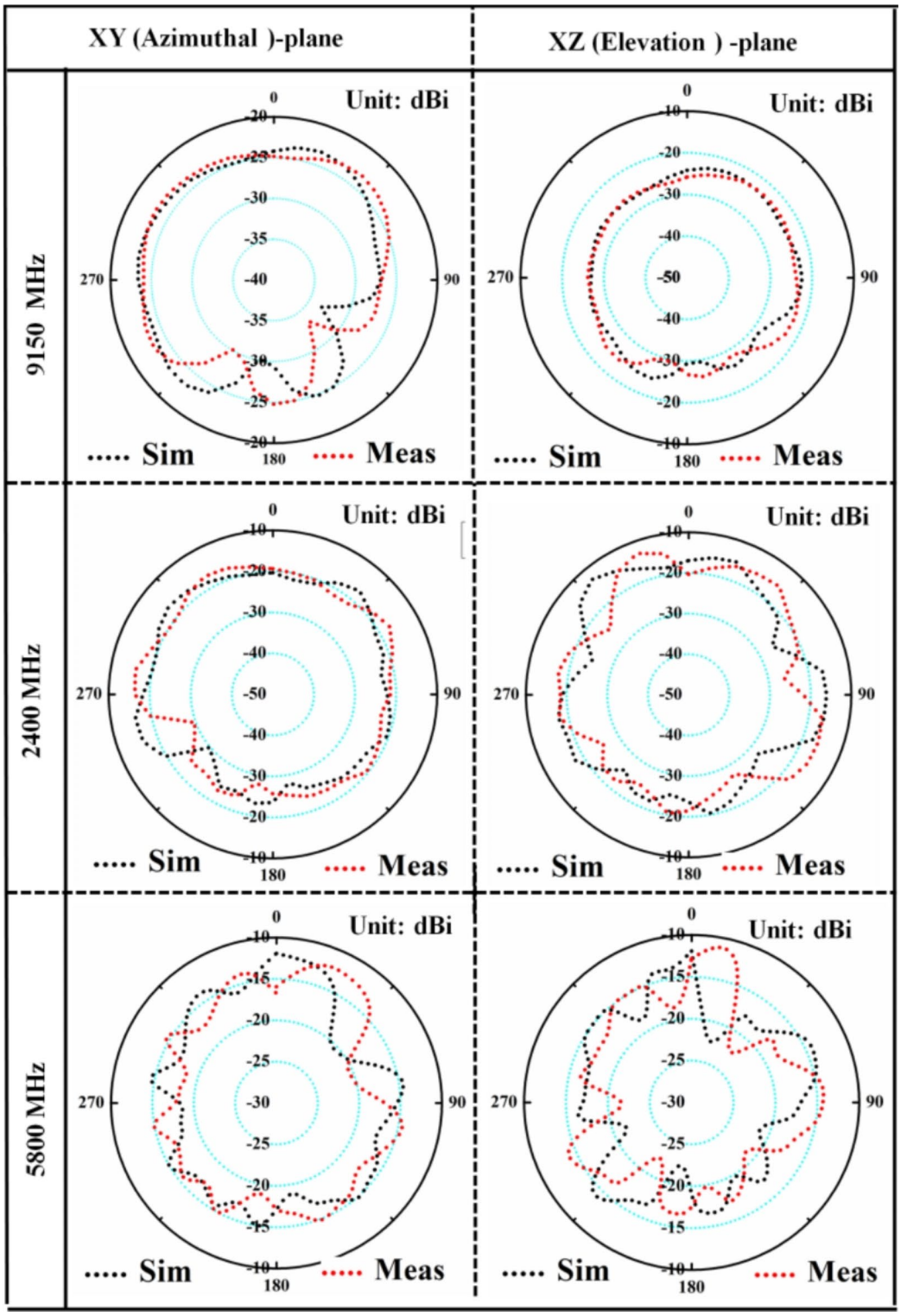

Fig. 14. Comparison of far field gain patterns of the designed extraoral integrated antenna in azimuthal (*phi* = 0˚) and elevation (*theta* = 90˚) planes at 915 MHz, 2400 MHz and 5800 MHz.

of 30 dBm at the higher ISM band frequencies of 2.45 GHz and 5.8 GHz[48]. It shows that the differentially driven extraoral integrated antenna can support transcieving safely at higher ISM band frequencies.

Link budget

The estimation of wireless data transmission link performance of the extraoral integrated antenna is carried out with respect to an external receiving unit. Here, we have estimated link budget parameter at two different data

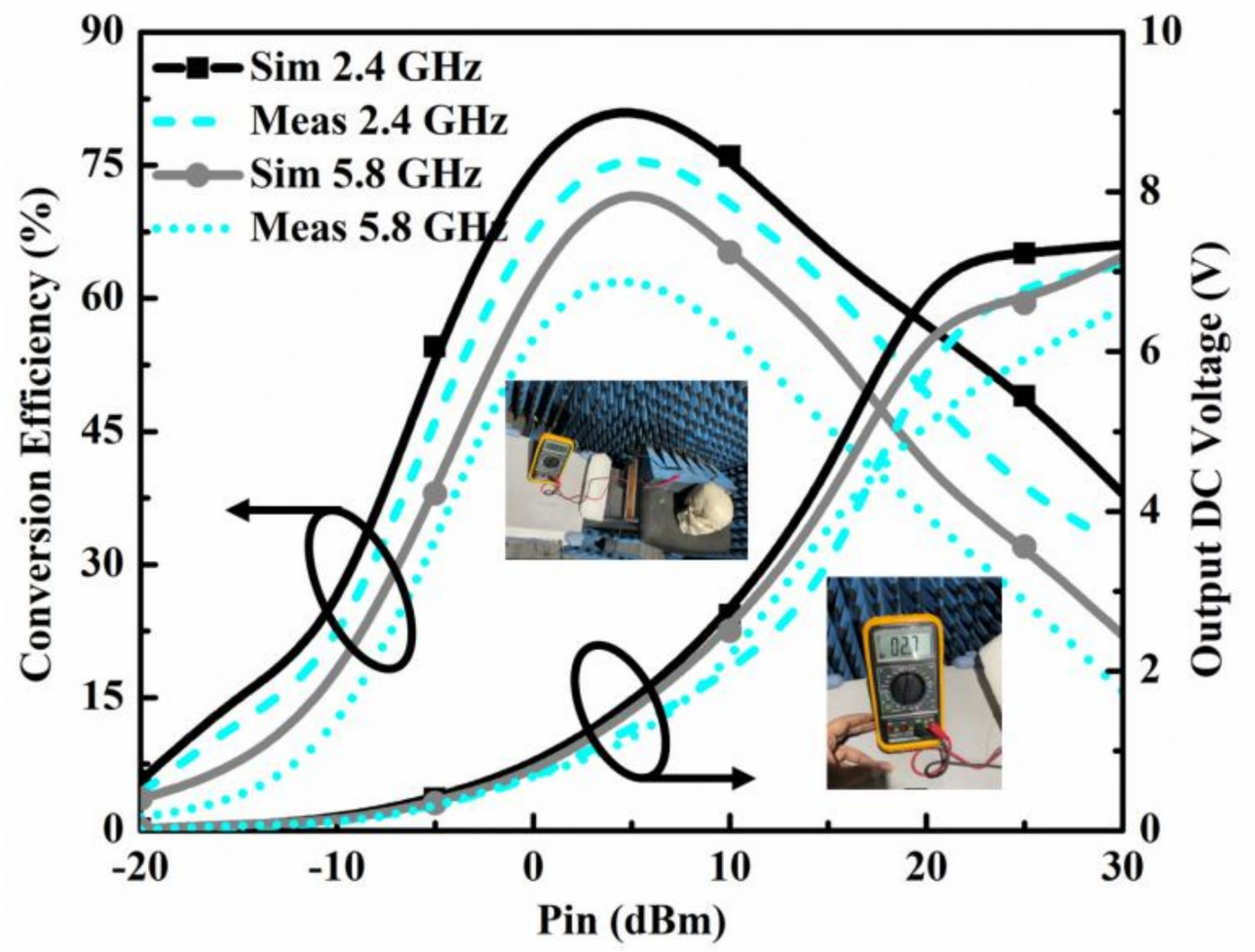

Fig. 15. Comparison of conversion efficiencies of differentially configured rectifier at both higher frequencies.

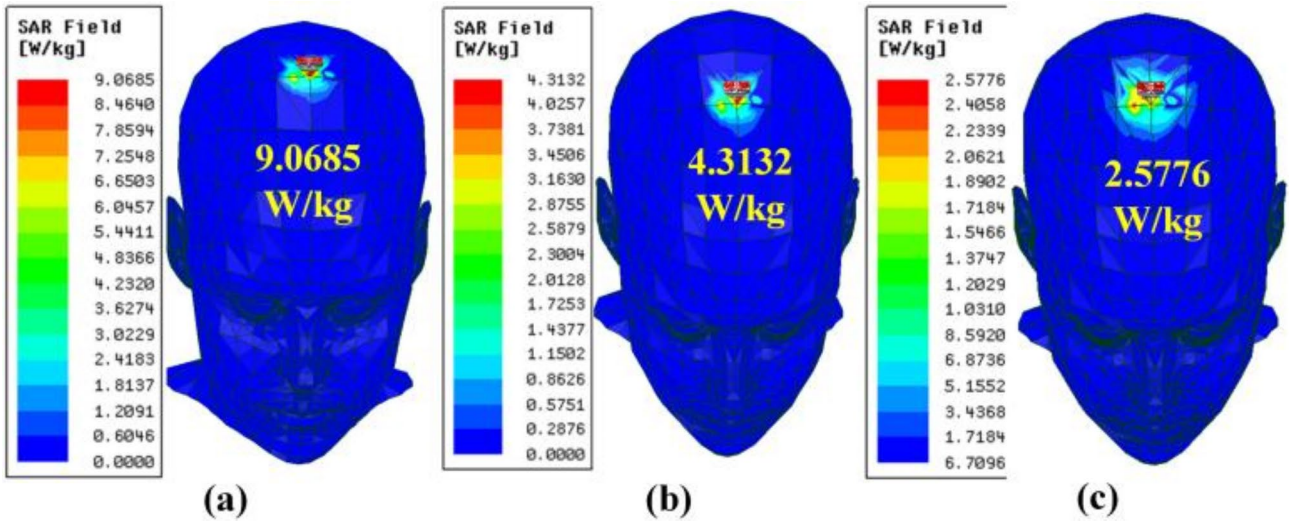

Fig. 16. Simulated averaged 1-g SAR distributions on the anatomical head model at (a) 915 MHz (b) 2400 MHz and (c) 5800 MHz.

rates (B_r), based on the equations reported in[49]. The input power to the extraoral antenna (P_t) is set at level of -16dBm, and gain of receiving dipole (G_r) is equal to 2.15dBi.

Table 3 presents all the variables related to transmitter, propagation medium, receiver and signal quality considered while evaluating the link margin at 0.915 GHz intended. In addition, considering the fact that the TDS antennas will be interfaced with dual port control unit (CC2510)[14,50], we further computed the link margin including the need of balun as interface.

This is presented in terms of additional Interface losses (IL), taken from[14]. Also, the antenna mismatch losses are included at the 0.915 GHz where the ML_{Tx} value of 0.017 dB is considered based the value of differential reflection coefficient[49]. The wireless RF telemetric link allows minimum margin of 10 dB required for reliable transmission[49,51]. Figure 17 illustrates that the differentially measuring extraoral antenna is well capable of sensing and transmitting the data rate of 24 Kbps over a distance 20 m by minimizing additional interface losses (IL) with high margin of 20 dB. For higher data rate of 250 Kbps, the maximum transmission distance is more than 25 m (approx.) with high margin of 20 dB. It could be possible due to the differential facing of the extraoral antenna that overcomes the additional losses due to the interfacing and matching circuitries, which can help to keep the eTDS circuitry intact. Hence, the designed differentially measuring extraoral integrated antenna effectively channelizes the sensor data to neighboring devices situated at a distance greater than 20 m, which is sufficient for eTDS technology related applications.

Conclusion

In this study, the performance of symmetrical differentially measuring extraoral antenna integrated with rectifier is evaluated that operates in the ISM bands at three frequencies of 915 MHz, 2400 MHz, and 5800 MHz with dual-mode transmission for eTDS technology-based applications. The triple band differential extraoral antenna is initially designed on a 0.254 mm thin, flexible substrate using Ansys HFSS18.0. The meander shaped patch, slots in ground, and two vias provided the symmetrically balanced configuration and significant miniaturization. Subsequently, the differentially driven rectifier is designed using the ADS simulator and coplanarly integrated on the same substrate using HFSS 18.0 simulator. Then, the differential rectenna performance was optimized to achieve the desired band resonating performances. Later, the performance of the extraoral differentially configured antenna and rectenna is measured and evaluated independently using an artificial human head model. The measurement values of -10 dB impedance bandwidth and far-field gain were 13.04% and −22.9 dBi, respectively, at 915 MHz; 8.61% and −14.16 dBi, respectively, at 2400 MHz; and 8.89% and −12.83 dBi respectively, at 5800 MHz. Minor distortions could be seen due to the fabrication tolerances and measurement accessories. The fabricated rectenna was given 11 dBm input power, and the corresponding DC output voltage of 2.70 V was measured through the load resistor. It is enough for sustaining the operation of the eTDS microcontroller unit and thus ensures the increased lifetime of the rechargeable batteries. Additionally, the sensed data transmission at the two data rates with a high input power of 22.45 dBm (without need of the matching circuits) is assessed without compromising the SAR safety levels. Thus, the differentially measuring extraoral antenna cascaded with coplanar rectifier validates its potential role for eTDS dual mode transfer support to nearby iOT-based devices.

Symbol	Variable	Value
Transmitter		
F_r (MHz)	Resonance frequency	915
P_t(dBm)	Transmitter power	−16
G_t (dBi)	Antenna gain	−22.36
EIRP	Effective isotropic radiated power	−38.36
ML_{TX}(dB)	Impedance mismatch loss	0.017
Propagation		
L_f (dB)	Free space loss	Distance variation
Receiver		
G_r (dBi) T_0 (Kelvin) K	Receiving Antenna gain Temperature Boltzmann constant	2.15 273 1.38E-23
N_0 (dB/Hz)	Noise power density	−203.9
Signal quality		
B_r (Kb/S)	Bit rate	250,24
E_b/N_0 (dB) G_c(dB) G_d (dB)	PSK modulation Coding gain Fixing deterioration gain	9.6 0 2.5

Table 3. Link budget calculation.

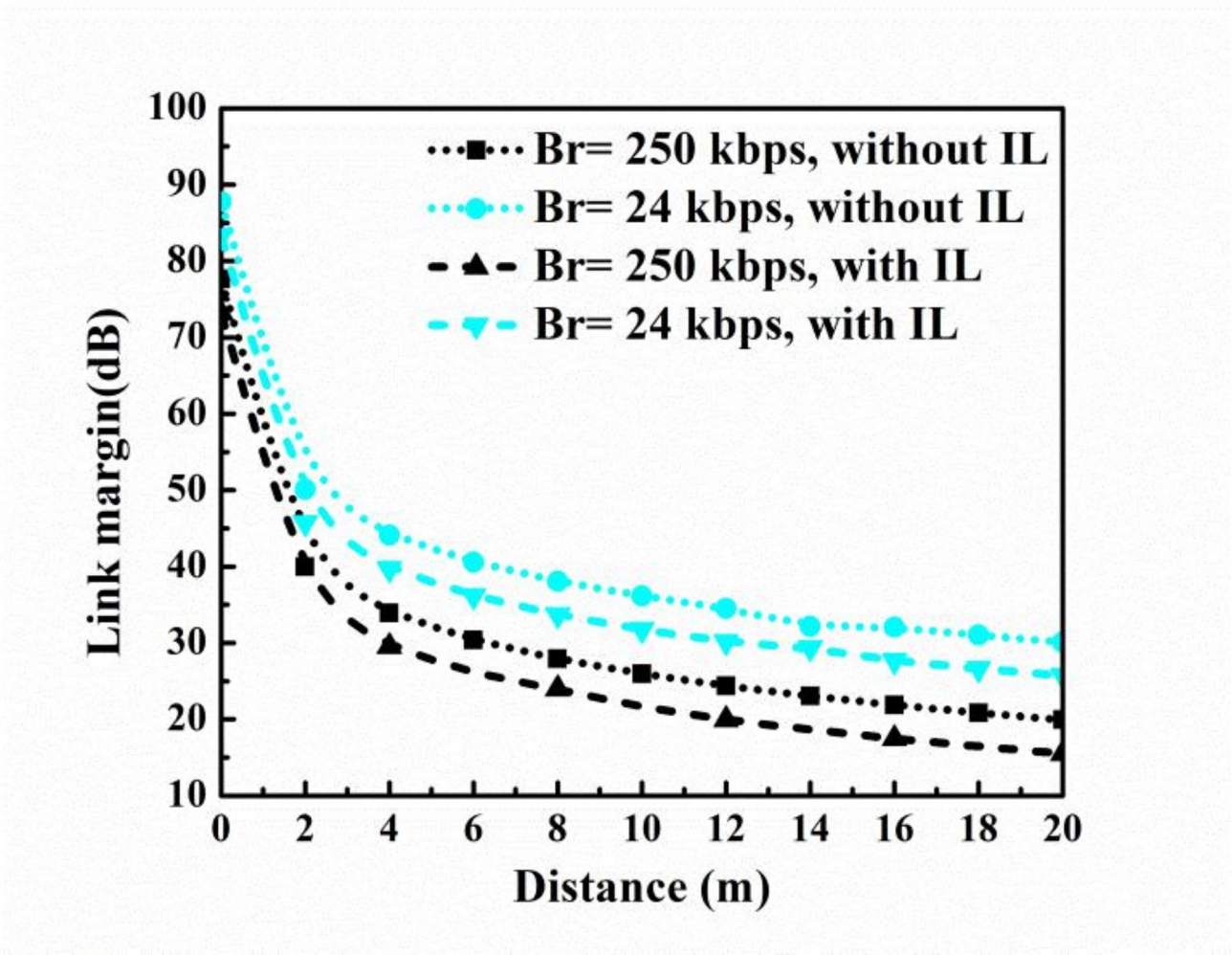

Fig. 17. Wireless telemetric link margin at 915.0 MHz.

Data availability

The datasets used and/or analysed during the current study are available from the corresponding author on reasonable request.

Received: 20 March 2024; Accepted: 30 September 2024
Published online: 22 October 2024

References

1. Kim, J. et al. Assessment of the tongue-drive system using a computer, a smartphone, and a powered-wheelchair by people with tetraplegia. *J. Spinal Cord Med.* **24**, 1–2 (2013).
2. Tejas, C., Tejashwini, V. & Murari, V. Assistive technology: An IoT based device for physically challenged people and hospital inmates. In *3rd IEEE Int. Conf. Recent Trends Electron. Inf. Commun. Technol. RTEICT 2018 - Proc.* 1906–1911. https://doi.org/10.1109/RTEICT42901.2018.9012369 (2018).
3. Jafari, A., Buswell, N., Ghovanloo, M. & Mohsenin, T. A. Low-power Wearable stand-alone Tongue Drive System for people with severe disabilities. *IEEE Trans. Biomed. Circuits Syst.* **12**, 58–67 (2018).
4. Huo, X. & Ghovanloo, M. Tongue drive: a wireless tongue-operated means for people with severe disabilities to communicate their intentions. *IEEE Commun. Mag.* **50**, 128–135 (2012).
5. Postolache, O. A., Girao, P. M. B. S., Mendes, J., Pinheiro, E. C. & Postolache, G. Physiological parameters measurement based on wheelchair embedded sensors and advanced signal processing. *IEEE Trans. Instrum. Meas.* **59**, 2564–2574 (2010).
6. San-Segundo, R., Echeverry-Correa, J. D., Salamea, C. & Pardo, J. M. Human activity monitoring based on hidden Markov models using a smartphone. *IEEE Instrum. Meas. Mag.* **19**, 27–31 (2016).
7. Nazemzadeh, P., Moro, F., Fontanelli, D., Macii, D. & Palopoli, L. Indoor positioning of a robotic walking assistant for large public environments. *IEEE Trans. Instrum. Meas.* **64**, 2965–2976 (2015).
8. Liao, L. et al. A novel 16-channel wireless system for electroencephalography measurements with dry spring-loaded sensors. *IEEE Trans. Instrum. Meas.* **63**, 1545–1555 (2014).
9. Tanimoto, Y., Nanba, K., Tokuhiro, A., Ukida, H. & Yamamoto, H. Measurement system of transfer motion for patients with spinal cord injuries. *IEEE Trans. Instrum. Meas.* **57**, 213–219 (2008).

10. Tanimoto, Y., Nanba, K., Director, A. T., Ukida, H. & Yamamoto, H. Measurement of wheelchair turn radius for SCI patient's remodeling house. *2009 IEEE Intrumentation Meas. Technol. Conf.* **I2MTC 2009**, 1352–1356. https://doi.org/10.1109/IMTC.2009.5168666 (2009).
11. Chandra, R. & Johansson, A. J. Antennas and propagation for in-mouth tongue-controlled devices in wireless body area networks. *IEEE Antennas Wirel. Propag. Lett.* **14**, 1518–1521 (2015).
12. Ahlawat, S., Kanaujia, B. K., Rambabu, K., Peter, I. & Matekovits, L. Circularly polarized differential intra-oral antenna design validation and characterization for tongue drive system. *Sci. Rep.* **13**, 1–18 (2023).
13. Andreasen Struijk, N. S. Development and functional demonstration of a wireless intraoral inductive tongue computer interface for severely disabled persons. *Disabil. Rehabil Assist. Technol.* **12**, 631–640 (2017).
14. Kong, F., Qi, C., Lee, H., Durgin, G. D. & Ghovanloo, M. Antennas for Intraoral Tongue Drive System at 2.4 GHz: design, characterization, and comparison. *IEEE Trans. Microw. Theory Tech.* **66**, 2546–2555 (2018).
15. Zada, M. & Yoo, H. Miniaturized dual band antennas for intra-oral tongue drive system in the ISM bands 433 MHz and 915 MHz: design, safety, and link budget considerations. *IEEE Trans. Antennas Propag.* **67**, 5843–5852 (2019).
16. Basir, A., Zada, M. & Yoo, H. Compact and flexible wideband antenna for intraoral tongue-drive system for people with disabilities. *IEEE Trans. Antennas Propag.* **68**, 2405–2409 (2020).
17. Kim, J. et al. Assessment of the tongue-drive system using a computer, a smartphone, and a powered-wheelchair by people with tetraplegia. *IEEE Trans. Neural Syst. Rehabil Eng.* **24**, 68–78 (2016).
18. Ahlawat, S., Singh, N., Kanaujia, B. K. & Rambabu, K. A. Dual band differential intraoral antenna and system for wireless data and radiative near-field power transfer. *IEEE Trans. Antennas Propag.* 1–1. https://doi.org/10.1109/tap.2022.3232723 (2023).
19. Iqbal, A. et al. Biotelemetry and wireless powering of biomedical implants using a rectifier integrated self-diplexing implantable antenna. *IEEE Trans. Microw. Theory Tech.* **69**, 3438–3451 (2021).
20. Iqbal, A., Al-Hasan, M., Mabrouk, I., Ben & Denidni, T. A. Wireless powering and telemetry of deep-body ingestible bioelectronic capsule. *IEEE Trans. Antennas Propag.* **70**, 9819–9830 (2022).
21. Duan, Z., Guo, Y. X., Xue, R. F., Je, M. & Kwong, D. L. Differentially fed dual-band implantable antenna for biomedical applications. *IEEE Trans. Antennas Propag.* **60**, 5587–5595 (2012).
22. Zhang, K. et al. A conformal differentially fed antenna for ingestible capsule system. *IEEE Trans. Antennas Propag.* **66**, 1695–1703 (2018).
23. Wang, H., Feng, Y. & Guo, Y. A. Differentially-fed antenna with complex impedance for ingestible wireless capsules. *IEEE Antennas Wirel. Propag. Lett.* **PP**, 1 (2021).
24. Ahlawat, S., Kanaujia, B. K. & Rambabu, K. Flexible and wearable dual-band differential extraoral antenna for eTDS applications. *IEEE J. Electromagn. RF Microwaves Med. Biol.* https://doi.org/10.1109/JERM.2023.3271459 (2023).
25. Liu, Y., Chen, Y., Lin, H. & Juwono, F. H. A novel differentially fed compact dual-band implantable antenna for biotelemetry applications. *IEEE Antennas Wirel. Propag. Lett.* **15**, 1791–1794 (2016).
26. Wang, H., Feng, Y. & Guo, Y. A. Differentially fed antenna with complex impedance for ingestible wireless capsules. *IEEE Antennas Wirel. Propag. Lett.* **21**, 139–143 (2022).
27. Shen, S., Chiu, C. Y. & Murch, R. D. A dual-port triple-band L-probe microstrip patch rectenna for ambient RF energy harvesting. *IEEE Antennas Wirel. Propag. Lett.* **16**, 3071–3074 (2017).
28. Aboualalaa, M., Mansour, I. & Pokharel, R. K. Energy harvesting rectenna using high-gain triple-band antenna for powering internet-of-things (IoT) devices in a Smart Office. *IEEE Trans. Instrum. Meas.* **72**, 1–12 (2023).
29. Iqbal, A., Sura, P. R., Al-Hasan, M., Mabrouk, I. B. & Denidni, T. A. Wireless power transfer system for deep-implanted biomedical devices. *Sci. Rep.* **12**, 1–13 (2022).
30. Sun, H. An enhanced rectenna using differentially-fed rectifier for wireless power transmission. *IEEE Antennas Wirel. Propag. Lett.* **15**, 32–35 (2016).
31. Chandravanshi, S., Sarma, S., Sen & Akhtar, M. J. Design of triple band differential rectenna for RF energy harvesting. *IEEE Trans. Antennas Propag.* **66**, 2716–2726 (2018).
32. De Donno, D., Catarinucci, L. & Tarricone, L. RAMSES: RFID augmented module for smart environmental sensing. *IEEE Trans. Instrum. Meas.* **63**, 1701–1708 (2014).
33. Verma, S., Rano, D., Malhotra, S. & Hashmi, M. S. Measurements and characterization of a newly developed novel miniature WIPT System. *IEEE Trans. Instrum. Meas.* **70**, 1–11. https://doi.org/10.1109/TIM.2021.3075537(2021).
34. Arrawatia, M., Baghini, M. S. & Kumar, G. Differential microstrip antenna for RF energy harvesting. *IEEE Trans. Antennas Propag.* **63**, 1581–1588 (2015).
35. Benassi, F., Paolini, G., Masotti, D. & Costanzo, A. A. Wearable flexible energy-autonomous filtenna for ethanol detection at 2.45 GHz. *IEEE Trans. Microw. Theory Tech.* **69**, 4093–4106 (2021).
36. Ullah, M. A. et al. A review on antenna technologies for ambient RF energy harvesting and wireless power transfer: designs, challenges and applications. *IEEE Access.* **10**, 17231–17267 (2022).
37. Sahadat, M. N., Alreja, A., Srikrishnan, P. & Ghovanloo, M. A multimodal human computer interface combining head movement, speech and tongue motion for people with severe disabilities. In *IEEE Biomed. Circuits Syst. Conf. Eng. Heal. Minds Able Bodies, BioCAS 2015 - Proc.* https://doi.org/10.1109/BioCAS.2015.7348317 (2015).
38. Huo, X., Wang, J. & Ghovanloo, M. A magneto-inductive sensor based wireless tongue-computer interface. *IEEE Trans. Neural Syst. Rehabil Eng.* **16**, 497–504 (2008).
39. Quddious, A. et al. Dual-band compact rectenna for UHF and ISM wireless power transfer systems. 1–6. https://doi.org/10.1109/TAP.2020.3025299 (2020).
40. High-impedance, W. S. A 5. 8-GHz Band Highly Efficient 1-W Rectenna. 1–9 (2021).
41. Chandravanshi, S. & Katare, K. K. A flexible dual-band rectenna with full azimuth coverage. **9**, (2021).
42. Stoecklin, S., Yousaf, A., Volk, T. & Reindl, L. Efficient wireless powering of biomedical sensor systems for multichannel brain implants. *IEEE Trans. Instrum. Meas.* **65**, 754–764 (2016).
43. Lin, Q. W. & Zhang, X. Y. *Ext. Input Power Range* **64**, 2943–2954 (2016).
44. Gabriel, C., Gabriel, S. & Corthout, E. The dielectric properties of biological tissues: I. Literature survey. *Phys. Med. Biol.* **41**, 2231–2249 (1996).
45. Basir, A. & Yoo, H. Efficient wireless power transfer system with a miniaturized quad-band implantable antenna for deep-body multitasking implants. *IEEE Trans. Microw. Theory Tech.* **68**, 1943–1953. https://doi.org/10.1109/TIM.2022.3185622 (2020).
46. Ahlawat, S. et al. Design and performance measurement of implantable differential integrated antenna for wireless biomedical instrumentation applications. *IEEE Trans. Instrum. Meas.* **71**, 1–10 (2022).
47. Gadhafi, R., Cracan, D., Mustapha, A. A. & Sanduleanu, M. An h-shaped differential fed patch antenna for a gan base station transmitter. *Prog Electromagn. Res. M.* **80**, 181–191 (2019).
48. Bercich, R. A., Duffy, D. R. & Irazoqui, P. P. Far-field RF powering of implantable devices: safety considerations. *IEEE Trans. Biomed. Eng.* **60**, 2107–2112 (2013).
49. Liu, C., Guo, Y. X. & Xiao, S. Capacitively loaded circularly polarized implantable patch antenna for ISM band biomedical applications. *IEEE Trans. Antennas Propag.* **62**, 2407–2417 (2014).
50. Park, H. & Ghovanloo, M. Wireless communication of intraoral devices and its optimal frequency selection. *IEEE Trans. Microw. Theory Tech.* **62**, 3205–3215 (2014).

51. Kong, F., Zada, M., Yoo, H. & Ghovanloo, M. Adaptive matching transmitter with dual-band antenna for intraoral tongue drive system. *IEEE Trans. Biomed. Circuits Syst.* **12**, 1279–1288 (2018).

Author contributions

A.S. conceived and performed the simulations, experiment, and drafted the manuscript. N.S. and A.M.Z. conducted the experiment. B.K.K. and K.R. analyzed the results. B.K.K. and L.M. have proofread the manuscript. L.M. supervised the overall work and provided funding for the experiments. All authors reviewed the manuscript.

Declarations

Competing interests

The authors declare no competing interests.

Additional information

Correspondence and requests for materials should be addressed to L.M.

Reprints and permissions information is available at www.nature.com/reprints.

Publisher's note Springer Nature remains neutral with regard to jurisdictional claims in published maps and institutional affiliations.